J. Fluid Mech. (1999), *vol.* 397, *pp.* 285–316. Printed in the United Kingdom

Generation of Tollmien–Schlichting waves by convecting gusts interacting with sound

By XUESONG WU

Department of Mathematics, Imperial College, 180 Queens Gate, London SW7 2BZ, UK

(Received 14 September 1998 and in revised form 25 May 1999)

A new mechanism is proposed for the generation of Tollmien–Schlichting (T–S) waves by free-stream turbulence. For definiteness and self-consistency, the mechanism is described mathematically by using a triple-deck formalism. The free-stream turbulence is represented by convecting gusts consisting of the so-called vortical and entropy waves of small amplitude. We show that suitable convecting gusts can interact with sound waves in the free stream to produce a forcing that has the same time and length scales as those of the T–S waves, thereby exciting such waves in the vicinity of the lower branch of the neutral stability curve. The T–S waves so produced have the order of magnitude of $\epsilon^2 R^{5/16}$, where ϵ is the amplitude of the free-stream disturbance and R the global Reynolds number. The scale conversion is achieved without resorting to any non-homogeneity on the wall, and hence the mechanism operates in a flat boundary layer. Furthermore, the T–S waves so generated do not undergo any immediate decay, as they may do in some other receptivity processes. For homogeneous isotropic free-stream turbulence, the spectrum of the T–S waves is obtained. The efficiency of the receptivity mechanism is assessed by parametric studies.

1. Introduction

Laminar–turbulent transition in a boundary layer is a complex process involving a sequence of linear and nonlinear events. The first of these is the so-called receptivity process (Morkovin 1969; Reshotko 1976), in which external disturbances present in the environment (e.g. in the free stream and/or on the wall) excite internal oscillations within the boundary layer. In the case of weak external disturbances, the internal oscillations propagate into the unstable region downstream, wherein they experience exponential amplification, and are called Tollmien–Schlichting (T–S) instability waves. The characteristics of the T–S waves, including their dispersion relation, the distribution normal to the wall and the amplification rate, can be well predicted by linear stability theory. Further downstream, nonlinear effects become significant, leading to the final breakdown of laminar flow. In the case where the external disturbance is sufficiently strong, the transition may occur prematurely without the involvement of the T–S waves.

One of the important experimental observations is that the transition location depends on the nature and intensity of the disturbance in the environment, in particular on the turbulence level in the free stream. Such a dependence has been attributed to the size of the initial instability waves that the external disturbances excite. The aim of receptivity study is to calculate this initial amplitude, which obviously cannot be provided by stability theory since the instability waves appear as

eigensolutions. It is known that the initial amplitude crucially affects the subsequent development. Clearly, for effective laminar-flow control, it is important to study the receptivity as well as the stability properties.

As was shown by Kovasznay (1953), within linear approximation a general small-amplitude unsteady disturbance in the free stream can be decomposed into three different types: acoustic, vortical and entropy modes. The first corresponds to the pressure fluctuation, which propagates through the fluid with the speed of sound. The latter two represent vorticity and temperature perturbations being convected by the free stream without causing pressure fluctuation. Because of this feature, they are usually referred to as convecting gusts. In many applications, they have been used to represent the free-stream turbulence. The length and time scales of each of these disturbances do not satisfy the dispersion relation of the T–S waves, and hence none of them alone is capable of generating T–S waves. Therefore the key issue of receptivity studies is to identify scale-conversion mechanisms, which 'tune' the time and/or length scales of the external disturbance so as to match those of the T–S waves.

Significant theoretical contributions were made by Goldstein (1983, 1985) and Ruban (1984), whose works were apparently stimulated by important experiments of Leehey & Shapiro (1980), Kachanov, Kozlov & Levchenko (1978) and Aizin & Polyakov (1979). All these investigations were concerned with *the receptivity due to acoustic disturbances*. Goldstein (1983) shows that the so-called Lam–Rott eigensolution (which can be excited by the sound interacting with the non-parallel mean flow near the leading edge) undergoes wavelength shortening under the influence of the non-parallel-flow effect and finally turns into T–S waves near the lower branch of the neutral curve. Further calculations of the T–S amplitude were performed by Goldstein, Sockol & Sanz (1983). This receptivity, however, is somewhat weak in the sense that the waves experience considerable decay before reaching their neutral-stability point. A more efficient mechanism was proposed independently by Goldstein (1985) and Ruban (1984). They show that the oscillatory flow driven by the sound wave interacts with a relatively rapid local variation in the mean flow induced by a small roughness (i.e. hump) on the wall, or sudden curvature change such as the one that occurs at the juncture of the leading-edge ellipse and the straight portion of the plate, to produce an unsteady forcing that takes on the frequency of the sound and the length scale of the local mean flow. Due to this forcing the T–S waves are generated in the unsteady scattered field. The coupling between the sound wave and the T–S waves is most efficient when the roughness or curvature change is near the lower branch, for which case the coupling coefficient is of order one. See also Goldstein & Hultgren (1987).

It became clear from the analyses of Goldstein and Ruban that in order for the acoustic disturbance to excite T–S waves, what is crucial is some form of short-scale variation (inhomogeneity) either in the mean flow or in the boundary conditions. In addition to the localized surface roughness, such inhomogeneity can be caused also by many other factors including marginal separation (Goldstein, Leib & Cowley 1987), local wall suction/blowing and change of wall admittance (Choudhari 1993, 1994). All the aforementioned theoretical studies except the last two adopted a high-Reynolds-number approach, reviews of which are given by Goldstein & Hultgren (1989) and Kozlov & Ryzhov (1990).

A finite-Reynolds-number approach based on the Orr–Sommerfeld (O–S) equation was formulated by Choudhari & Streett (1992) and Crouch (1992). Some earlier work by Russian researchers can be found in Zhigulev & Tumin (1987). This method

retains the essence of the Goldstein–Ruban theory, but uses inhomogeneous O–S equations rather than the triple-deck equations to compute the mean-flow distortion as well as the resultant T–S waves. The same method has been employed to study the receptivity due to distributed roughness. Given the success of the O–S equation in predicting the linear growth rate of T–S waves, it has been hoped that this approach, in spite of its inherent inconsistency, may lead to more accurate results for receptivity problems. However, the finite-Reynolds-number approach has other limitations. For instance it cannot be applied to the receptivity problem of marginal separating flow or to the case where the roughness is large, because in both cases the mean-flow distortions become nonlinear, and must be described by the triple-deck approach. Roughness of large size was tackled numerically by Bodonyi *et al.* (1989). Recently, Hammerton & Kerschen (1996, 1997) and Haddad & Corke (1998) investigated the effect of leading-edge bluntness on the efficiency of receptivity. More recent experiments include Saric, Wei & Rasmussen (1995), Kobayashi *et al.* (1995) and Kosorygin, Radeztsky & Saric (1995). In the first of these papers, quantitative comparisons were made with existing theory for the leading-edge acoustic receptivity, while the last two studied the interference between the T–S waves generated by the leading edge and multi-roughness elements.

Despite its importance, the role of *vortical disturbances* in the generation of T–S waves is less well understood. As stated above, this type of mode is not associated with any pressure gradient, and hence does not penetrate into the boundary layer in the sense that its signature is exponentially small there as was shown mathematically by Gulyaev *et al.* (1989). Based on this and the fact that the local mean-flow variation produced by a roughness concentrates in the region near the wall, one might conclude that vortical disturbances are unable to excite T–S waves. Such a conclusion was found to be somewhat premature by Duck, Ruban & Zhikharev (1996), who investigated this receptivity process using a triple-deck approach. They observe that the roughness-induced mean flow outside the boundary layer, though of relatively small magnitude, does not vanish completely. So it can interact with the vortical disturbance to generate T–S waves (see also Kerschen 1991). The coupling coefficient, is a factor of $R^{-1/8}$ smaller than that in the corresponding acoustic case. For a typical Reynolds number $R = 10^6$, this means that the amplitude of the T–S wave is $\frac{1}{6}$ of that generated by the sound. Calculations using an O–S approach estimate that the coupling is even weaker (Crouch 1994), although it improves for the three-dimensional, low-frequency vortical gust (Choudhari 1996). Exist-ing theoretical results therefore do not seem to comply fully with the general expectation that the vortical disturbance ought to be an efficient T–S wave generator as can be inferred from the experimental evidence that the transition location depends strongly on the turbulence level (as well as on other factors such as wall roughness). Ryzhov & Timofeev (1995) investigated the generation of the wavepackets by the interaction of a line vortex with a local surface roughness.

Experiments on receptivity to vortical disturbances have proved to be more challenging than those on acoustic perturbations. It is very hard to control and quantify the vortical disturbances because of their random nature. Any T–S waves that they may produce are usually obscured by the broadband response of the boundary layer, especially by the large-amplitude, low-frequency components, i.e. the so-called 'Klebanoff modes' (see e.g. Kendall 1985; Westin *et al.* 1994 and references therein). Indeed, when the turbulence level is high, the Klebanoff mode may lead to bypass transition while the energy in the T–S frequency band appears relatively small. Nevertheless, the experiment of Kendall (1990) provided *direct* evidence for the generation

of T–S waves in the form of packets on a nominally flat-plate boundary layer, and established their role in the transition process. But the mechanism of their generation is still unclear. In the course of revising the present paper, we note that Dietz (1999) has successfully conducted controlled experiments, in which a single-frequency gust is generated by using a vibrating ribbon in the free stream. His experiments provide for the first time quantitative data regarding the initial amplitude of T–S waves generated by a convecting gust interacting with a wall roughness element.

In this paper, we shall propose a new mechanism for the generation of T–S waves by the free-stream turbulence. It involves the direct interaction between a convecting gust and a sound wave of suitable frequencies and wavenumbers so as to achieve scale conversion. Unlike the mechanism in the Goldstein–Ruban theory, the conversion of the external scales does not require any form of non-homogeneity on the wall or in the mean flow. Given that both the acoustic and vortical disturbances are always present in the free stream, this new mechanism (like the leading-edge mechanism) seems particularly pervasive, operating even in the simplest flows such as the flat boundary layer.†

The rest of the paper is organized as follows. The problem is formulated in § 2, where we first explain the physical idea in our receptivity mechanism without relying on mathematical details (§ 2.1). This is followed by specifying the necessary asymptotic scalings so as to describe the mechanism in the framework of the triple-deck approach. The dominant interaction takes place in the upper deck, and this is analysed in § 2.2. We show that the pressure at the quadratic order satisfies a Poisson equation (or an inhomogeneous wave equation in the supersonic regime), and contains the signature bearing the T–S wave scales. The forcing in the upper deck is transmitted, via the middle deck, to the lower deck, which is considered in § 3. We show that the boundary-layer equations in the lower deck couple to the Poisson (or the forced wave) equation to form an inhomogeneous system. Since its forcing term is in resonance with its eigenmode – the T–S wave – this system has a solution only if the T–S wave solution is included at a suitable lower order. The necessary solvability condition then determines the amplitude equation of the generated T–S wave. The solution to the amplitude equation enables us to introduce an appropriate coupling coefficient in § 4, where the receptivity process is discussed in detail by examining how the T–S waves develop from the upstream response. In § 5, we consider the generation of T–S waves by homogeneous free-stream turbulence. By a suitable superposition of the solution for each Fourier mode, we calculate the spectrum of the T–S waves in terms of those of the external turbulence. The efficiency of the coupling is assessed by parametric studies in § 6.

2. Formulation and scalings

We consider the two-dimensional compressible boundary layer over a semi-infinite flat plate. The oncoming flow is assumed to be uniform with velocity U_∞, perturbed by three-dimensional small-amplitude disturbances. The mean density, temperature and sound speed in the free stream are denoted by ρ_∞, T_∞ and a_∞ respectively. The unsteady disturbance will be specified later. We define the Reynolds number

$$R = U_\infty l/\mu_\infty$$

† This result, however, should not be interpreted as implying that surface roughness is unimportant. In fact it has been well established that transition process is extremely sensitive to the surface quality.

and the Mach number

$$M = U_\infty / a_\infty,$$

where l is the typical distance from the leading edge to the location where the receptivity commences. We assume that M is of $O(1)$ and covers both the subsonic ($M < 1$) and supersonic ($M > 1$) regimes. In the former regime, the viscous T–S instability is the only possible instability. In the supersonic regime, the T–S waves persist provided that they are sufficiently oblique (Smith 1989). The flow now also supports inviscid Rayleigh instability waves, which have asymptotically larger growth rates. However, in the low-Mach-number supersonic range, the oblique T–S waves appear to have the largest growth rate in numerical sense (Mack 1984), and therefore continue to play an important role in transition. Even in the fairly high-Mach-number regime, the generation of T–S waves may still be relevant because the T–S waves are the first to be excited by the external disturbance. They then evolve into inviscid Rayleigh waves as the upper branch of the neutral curve is approached.

The flow is to be described in the Cartesian coordinate system (x, y, z), with its origin at the leading edge, where x and y are along and normal to the plate respectively, and z is in the spanwise direction; they are non-dimensionalized by l. The time variable t is normalized by l/U_∞. The velocity (u, v, w), density ρ, temperature T, pressure p, and shear and bulk viscosities μ and μ' are non-dimensionalized by U_∞, ρ_∞, T_∞, $\rho_\infty U_\infty^2$ and μ_∞ respectively.

The fluid is assumed to be a perfect gas with a constant ratio of specific heats, γ. The governing equations of the flow are

$$\frac{\partial \rho}{\partial t} + \nabla \cdot (\rho \boldsymbol{u}) = 0, \tag{2.1}$$

$$\rho \frac{\mathrm{D}\boldsymbol{u}}{\mathrm{D}t} = -\nabla p + \frac{1}{R}\nabla \cdot (2\mu \mathbf{e}) + \nabla\big((\mu' - \tfrac{2}{3}\mu)\nabla \cdot \boldsymbol{u}\big), \tag{2.2}$$

$$\rho \frac{\mathrm{D}T}{\mathrm{D}t} = (\gamma - 1)M^2 \frac{\mathrm{D}p}{\mathrm{D}t} + \frac{1}{P_r R}\nabla \cdot (\mu \nabla T) + \frac{(\gamma - 1)M^2}{R}\Phi, \tag{2.3}$$

$$\gamma M^2 p = \rho T, \tag{2.4}$$

where $\mathbf{e}$ and Φ represent the tensor of the strain rate and the dissipation function:

$$e_{ij} = \frac{1}{2}\left(\frac{\partial u_i}{\partial x_j} + \frac{\partial u_j}{\partial x_i}\right), \quad \Phi = 2\mu \mathbf{e} : \mathbf{e} + (\mu' - \tfrac{2}{3}\mu)(\nabla \cdot \boldsymbol{u})^2,$$

and P_r is the Prandtl number. The shear viscosity μ depends on the temperature T, but the viscosity law does not affect the result of the present paper because the T–S instability, to leading order, is controlled by the wall shear, and does not depend on the detailed profile of the boundary layer flow.

2.1. *The physical idea*

Let us first explain the basic idea of our receptivity mechanism in fairly general terms before presenting it in the mathematical framework of a triple deck.

Suppose that a sound wave and a convecting gust are present in the free stream, and can be represented by

$$\epsilon_s \, \mathrm{e}^{\mathrm{i}(\alpha_s x - \omega_s t)} \quad \text{and} \quad \epsilon_c \, \mathrm{e}^{\mathrm{i}(\alpha_c x - \omega_c t)}$$

respectively, where ϵ_s (ϵ_c), α_s (α_c) and ω_s (ω_c) denote the amplitude, wavenumber and frequency of the sound (gust) respectively. For simplicity of illustration, here

we have taken the disturbances to be two-dimensional and also implicitly assumed that the sound propagates downstream in the streamwise direction, although these restrictions will be relaxed later on. At leading order the acoustic and vortical modes are independent, with each being governed by a set of linear equations (see e.g. Kovasznay 1953), which show that

$$\alpha_s = M\omega_s/(1+M), \quad \alpha_c = \omega_c. \tag{2.5}$$

At the quadratic order, the two waves can interact with each other. This produces a forcing proportional to

$$\exp \mathrm{i}\{(\alpha_c \pm \alpha_s)x - (\omega_c \pm \omega_s)t\}.$$

In a strictly uniform flow, the secondary flow due to the mutual interaction, which acts to mediate the energy transfer between different modes, can be calculated by a regular perturbation procedure, as was highlighted by Chu & Kovasznay (1958). However, in a shear flow which supports instability waves such as T–S waves, the situation is more interesting and intriguing in that the mutual interaction may lead to excitation of the eigenmodes. To see this point, let us suppose that the dispersion relation of the T–S waves is

$$F(\omega_{TS}, \alpha_{TS}, R; M) = 0 \tag{2.6}$$

which relates the frequency ω_{TS} and the wavenumber α_{TS} at a given Reynolds number R. In general for a given frequency ω, the wavenumber $\alpha_{TS} = \alpha_r + \mathrm{i}\alpha_i$ is a complex number except at the neutral Reynolds number R_c. Now if

$$\omega_c - \omega_s = \omega_{TS}, \quad \alpha_c - \alpha_s = \mathrm{Re}\,(\alpha_{TS}), \tag{2.7}$$

the response to the forcing would be similar to, but not exactly the same as, the T–S wave when $R \neq R_c$. The magnitude of the response is of order $\epsilon_s\epsilon_v$. When $R \approx R_c$, the relations (2.7) guarantee the resonant condition between the forcing and the T–S wave, leading to the generation of the latter. Mathematically, the resonant condition means that in order for the inhomogeneous system at the quadratic order to have an acceptable solution, the T–S wave must be included in the expansion at a suitable lower order.

The idea is in the same spirit as that of Luo & Zhou (1987), who were the first to propose that the interaction of two disturbances in the free stream may excite T–S waves in a flat boundary layer if the differences in their wavenumbers and frequencies satisfy the dispersion relation (2.6). However, in Luo & Zhou's model, the two participating disturbances were specified arbitrarily. This unfortunately makes their model artificial because the free-stream disturbance must be a combination of convecting gust and acoustic modes, each of which has its own dispersion relation such as (2.5).

The physical idea of our receptivity mechanism clearly applies to three-dimensional disturbances, and indeed the inclusion of three-dimensionality is crucial for the generation of T–S waves in the supersonic regime. In the following we shall take convecting gusts to be three-dimensional while the acoustic perturbation is two-dimensional. This choice is based on two obvious reasons: first, in any controlled experiments, it is much easier to introduce a planar sound than a two-dimensional gust; secondly in 'natural' situations, the oncoming gusts are most likely to be three-dimensional. As will become clear later, the above choice eventually allows us to consider the interaction between a sound wave and isotropic turbulence.

2.2. *Asymptotic scalings*

We now present the above mechanism on a quantitative basis. Although this could be done by using the O–S equation, we shall adopt the triple-deck formalism because first it is the appropriate mathematical framework describing the T–S waves; secondly it conveniently accommodates the interaction between the free-stream disturbances, as we shall see; thirdly and perhaps most importantly, the non-parallel effect, which plays a key rôle in the present mechanism, can be accounted for in a consistent manner only by a high-Reynolds-number asymptotic approach. In contrast, a finite-Reynolds-number approach would have to make use of a somewhat *ad hoc* approximation in order to include this effect.

For the lower-branch T–S waves, the frequency and wavelength scale with the Reynolds number as $\omega_{TS} = R^{2/8}\hat{\omega}_{TS}$, $\alpha_{TS} = R^{3/8}\hat{\alpha}_{TS}$. Such a scaling applies to both subsonic (Terent'ev 1981) and supersonic regimes (Smith 1989) except at transonic speeds. It follows from (2.5) and (2.7) that in order for the resulting forcing to have the same length and time scales as the T–S waves, it is necessary for the wavenumbers of both the convecting gust and the acoustic mode, α_c, β (the spanwise wavenumber) and α_s, to be of $O(R^{3/8})$. Their frequencies, ω_c and ω_s say, would be of this order since their phase velocities are of $O(1)$. The above considerations suggest the following scaling for the wavenumbers and the frequencies:

$$\alpha_c = R^{3/8}\hat{\alpha}_c, \quad \alpha_s = R^{3/8}\hat{\alpha}_s, \quad \beta = R^{3/8}\hat{\beta}; \quad \omega_c = R^{3/8}\hat{\omega}_c, \quad \omega_s = R^{3/8}\hat{\omega}_s, \tag{2.8}$$

in accordance with which we introduce the time, the streamwise and spanwise variables

$$\bar{t} = R^{3/8}t, \quad \bar{x} = R^{3/8}x, \quad \bar{z} = R^{3/8}z. \tag{2.9}$$

While the convecting gust and the acoustic mode both have relatively high frequencies, the difference of their frequencies must be relatively small so as to coincide with that of the T–S waves, i.e. $\omega_c - \omega_s = O(R^{-1/8}\omega_c)$, which can be more precisely expressed in terms of the rescaled frequencies as

$$\hat{\omega}_c - \hat{\omega}_s = R^{-1/8}\hat{\omega}_{TS}. \tag{2.10}$$

Upstream of the neutral point, x_0 say, of the T–S wave with the rescaled frequency $\hat{\omega}_{TS}$, the quadratic interaction generates a small-amplitude response. But in the vicinity of x_0, the forcing becomes in resonance with the T–S wave if the condition

$$\hat{\alpha}_c - \hat{\alpha}_s = \hat{\alpha}_{TS} \tag{2.11}$$

is satisfied, where $\hat{\alpha}_{TS}$ is the neutral wavenumber of the T–S wave. On approaching x_0, the forced response tends to infinity in magnitude, and takes on the characteristics of the T–S wave. It may be expected that the forced response upstream eventually evolves into the T–S wave after going through the resonance. In order to describe this crucial process and also to obtain the uniformly valid solution near x_0, it is necessary to include the non-parallel flow effect, which becomes important in an $O(R^{-3/16})$ neighbourhood of x_0 (Ruban 1983; Hall & Smith 1984). So we introduce

$$x_1 = (x - x_0)/R^{-3/16}. \tag{2.12}$$

The amplitude of the T–S wave will be a function of x_1, and matches to the forced response upstream as $x_1 \to -\infty$. In the $x_1 = O(1)$ region, the variation of the growth rate with the streamwise position occurs at the same scale as the amplitude. This non-parallelism underpins the matching between the forced response and the T–S waves; see § 4 and figure 1. The importance of the $O(R^{-3/16})$ vicinity of the neutral

point was also noted by Choudhari (1993) in his study of the receptivity due to distributed roughness. However the scaling there is somewhat blurred as the analysis is based on a finite-Reynolds-number approach.

It follows from (2.9) and (2.12) that

$$\frac{\partial}{\partial t} \to R^{3/8}\frac{\partial}{\partial \bar{t}}, \quad \frac{\partial}{\partial x} \to R^{3/8}\frac{\partial}{\partial \bar{x}} + R^{3/16}\frac{\partial}{\partial x_1}, \quad \frac{\partial}{\partial z} \to R^{3/8}\frac{\partial}{\partial \bar{z}}. \tag{2.13}$$

The flow is described by the standard triple-deck structure consisting of the upper, main and lower decks. The procedure of determining the amplitude of the T–S wave is similar to those in weakly nonlinear theory (cf. Hall & Smith 1982, 1984).

The mean flow is taken to be the Blasius boundary layer, the profile of which is $U(\tilde{Y})$ ($\tilde{Y} = R^{1/2}y$). As $\tilde{Y} \to 0$,

$$U(\tilde{Y}) \to \lambda \tilde{Y}$$

where the skin friction

$$\lambda = \chi x^{-1/2} \quad \text{with} \quad \chi \approx 0.332. \tag{2.14}$$

We further expand λ about x_0, the location where the T–S wave becomes neutral,

$$\lambda = \lambda_0 + R^{-3/16}\lambda_1 x_1, \quad \text{with} \quad \lambda_1 = -\tfrac{1}{2}\chi x_0^{-3/2}. \tag{2.15}$$

2.3. *Upper deck and nonlinear interaction*

In the upper deck, the transverse variable is $\bar{y} = R^{3/8}y$ and the expansion takes form

$$\boldsymbol{u} = (1, 0, 0) + \epsilon \boldsymbol{u}_1 + \epsilon^2 R^{3/16}(\boldsymbol{u}_{TS}E + \text{c.c.}) + \epsilon^2 \boldsymbol{u}_2 + \cdots, \tag{2.16}$$

$$p = \frac{1}{\gamma M^2} + \epsilon p_1 + \epsilon^2 R^{3/16}(p_{TS}E + \text{c.c.}) + \epsilon^2 p_2 + \cdots, \tag{2.17}$$

$$T = 1 + \epsilon \tau_1 + \epsilon^2 R^{3/16}(\tau_{TS}E + \text{c.c.}) + \epsilon^2 \tau_2 + \cdots, \tag{2.18}$$

$$\rho = 1 + \epsilon \rho_1 + \epsilon^2 R^{3/16}(\rho_{TS}E + \text{c.c.}) + \epsilon^2 \rho_2 + \cdots, \tag{2.19}$$

where

$$E = \exp\{\mathrm{i}(\hat{\alpha}_{TS}\bar{x} + \hat{\beta}\bar{z} - R^{-1/8}\hat{\omega}_{TS}\bar{t})\},$$

and a bold letter denotes a vector. The $O(\epsilon)$ terms represent the unsteady disturbance in the free stream. We have assumed that the vortical and acoustic modes have the same order of magnitude, i.e. $\epsilon_s = \epsilon_c \equiv \epsilon$. This would not cause any loss of generality because the self-nonlinearity of each mode does not come into play to the order of our interest. Substitution of these expansions into (2.1)–(2.4) yields, at $O(\epsilon)$, the equations

$$\left(\frac{\partial}{\partial \bar{t}} + \frac{\partial}{\partial \bar{x}}\right)\rho_1 + \nabla \cdot \boldsymbol{u}_1 = 0, \tag{2.20}$$

$$\left(\frac{\partial}{\partial \bar{t}} + \frac{\partial}{\partial \bar{x}}\right)\boldsymbol{u}_1 = -\nabla p_1, \tag{2.21}$$

$$\left(\frac{\partial}{\partial \bar{t}} + \frac{\partial}{\partial \bar{x}}\right)\tau_1 = (\gamma - 1)M^2\left(\frac{\partial}{\partial \bar{t}} + \frac{\partial}{\partial \bar{x}}\right)p_1, \tag{2.22}$$

$$\gamma M^2 p_1 = \tau_1 + \rho_1. \tag{2.23}$$

We remind the reader that hereafter operators such as ∇, ∇^2 are defined with respect to the scaled variables $\bar{x}$, $\bar{y}$ and $\bar{z}$. The velocity and temperature may be eliminated

from (2.20)–(2.23) to obtain a single equation for the pressure p_1

$$M^2\left(\frac{\partial}{\partial\bar{t}}+\frac{\partial}{\partial\bar{x}}\right)^2 p_1-\nabla^2 p_1=0. \tag{2.24}$$

Equations (2.20)–(2.23) are subject to the boundary condition $v_1=0$ at $\bar{y}=0$. The solution can be expressed as a sum of convecting gust and acoustic modes (Kovasznay 1953),

$$\boldsymbol{u}_1=\boldsymbol{u}^{(s)}+\boldsymbol{u}^{(c)}, \tag{2.25}$$

$$p_1=p^{(s)}+p^{(c)},\quad \tau_1=\tau^{(s)}+\tau^{(c)},\quad \rho_1=\rho^{(s)}+\rho^{(c)}, \tag{2.26}$$

where the suffices s and c refer to the sound and convecting gust respectively. The acoustic mode is taken to be two-dimensional, and the solution has the form

$$\boldsymbol{u}^{(s)}=\hat{\boldsymbol{u}}_s\,\mathrm{e}^{\mathrm{i}\hat{\alpha}_s(\bar{x}-c\bar{t})}+\text{c.c.},\quad p^{(s)}=p_s\,\mathrm{e}^{\mathrm{i}\hat{\alpha}_s(\bar{x}-c\bar{t})}+\text{c.c.}, \tag{2.27}$$

and similar expressions hold for $\tau^{(s)}$ and $\rho^{(s)}$. By substituting $p^{(s)}$ into (2.24), the phase speed c is found to be

$$c=1\pm\frac{1}{M\cos\theta}\quad\text{with}\quad \cos\theta=\hat{\alpha}_s/(\hat{\alpha}_s^2+\hat{\beta}_s^2)^{1/2}. \tag{2.28}$$

Since θ is in the range $(-\pi,\pi)$, we can take the '+' sign without losing generality. It follows from (2.20)–(2.23) that

$$p_s=p_a(\mathrm{e}^{\mathrm{i}\hat{\beta}_s\bar{y}}+\mathrm{e}^{-\mathrm{i}\hat{\beta}_s\bar{y}}), \tag{2.29}$$

$$\rho_s=M^2p_a(\mathrm{e}^{\mathrm{i}\hat{\beta}_s\bar{y}}+\mathrm{e}^{-\mathrm{i}\hat{\beta}_s\bar{y}}),\quad \tau_s=(\gamma-1)M^2p_a(\mathrm{e}^{\mathrm{i}\hat{\beta}_s\bar{y}}+\mathrm{e}^{-\mathrm{i}\hat{\beta}_s\bar{y}}); \tag{2.30}$$

$$u_s=M\cos\theta\,p_a(\mathrm{e}^{\mathrm{i}\hat{\beta}_s\bar{y}}+\mathrm{e}^{-\mathrm{i}\hat{\beta}_s\bar{y}}),\quad v_s=M\sin\theta\,p_a(\mathrm{e}^{\mathrm{i}\hat{\beta}_s\bar{y}}-\mathrm{e}^{-\mathrm{i}\hat{\beta}_s\bar{y}}). \tag{2.31}$$

Note that the reflected wave has been included in order to satisfy the no-penetration condition at the wall.

The convecting gust propagates with the free stream, and so in general its solution can be represented as a supposition of the Fourier mode of $\mathrm{e}^{\mathrm{i}\hat{\alpha}_c(\bar{x}-\bar{t})+\mathrm{i}\hat{\beta}\bar{z}}$. For simplicity, we consider only one Fourier component in the gust so that in the far field (i.e. $\bar{y}\to\infty$), the vorticity and temperature fluctuations are

$$\begin{Bmatrix}\Omega_\infty^{(c)}\\ \tau_\infty^{(c)}\end{Bmatrix}=\begin{Bmatrix}\Omega_\infty\\ \tau_\infty\end{Bmatrix}\exp\{\mathrm{i}\hat{\alpha}_c(\bar{x}-\bar{t})+\mathrm{i}\hat{\beta}_v\bar{y}+\mathrm{i}\hat{\beta}\bar{z}\}. \tag{2.32}$$

The solution in the $\bar{y}=O(1)$ region can be sought of the form

$$\boldsymbol{u}^{(c)}=\hat{\boldsymbol{u}}_c(\bar{y})\,\mathrm{e}^{\mathrm{i}\hat{\alpha}_c(\bar{x}-\bar{t})+\mathrm{i}\beta\bar{z}}+\text{c.c.}, \tag{2.33}$$

and $\tau^{(c)}$ and $\rho^{(c)}$ have similar form, while $p^{(c)}=0$ as is implied by (2.21). We find that the components of the gust velocity vector $\hat{\boldsymbol{u}}_c$ are given by

$$\left.\begin{aligned}\hat{u}_c&=u_\infty\,\mathrm{e}^{\mathrm{i}\hat{\beta}_v\bar{y}}+(\mathrm{i}\hat{\alpha}_c/\hat{\gamma})v_\infty\,\mathrm{e}^{-\hat{\gamma}\bar{y}},\\ \hat{v}_c&=v_\infty(\mathrm{e}^{\mathrm{i}\hat{\beta}_v\bar{y}}-\mathrm{e}^{-\hat{\gamma}\bar{y}}),\\ \hat{w}_c&=w_\infty\,\mathrm{e}^{\mathrm{i}\hat{\beta}_v\bar{y}}+(\mathrm{i}\hat{\beta}/\hat{\gamma})v_\infty\,\mathrm{e}^{-\hat{\gamma}\bar{y}},\end{aligned}\right\} \tag{2.34}$$

where $\hat{\gamma}=(\hat{\alpha}_c^2+\hat{\beta}^2)^{1/2}$, and $\boldsymbol{u}_\infty\equiv(u_\infty,v_\infty,w_\infty)$ is related to Ω_∞ by the relation

$$\boldsymbol{u}_\infty=\frac{\mathrm{i}}{\hat{\gamma}^2}\hat{\boldsymbol{k}}\times\Omega_\infty,\quad \hat{\boldsymbol{k}}\equiv(\hat{\alpha}_c,\hat{\beta}_v,\hat{\beta}).$$

It follows immediately that $\hat{\boldsymbol{k}} \cdot \boldsymbol{u}_\infty = 0$, i.e.

$$\hat{\alpha}_c u_\infty + \hat{\beta}_v v_\infty + \hat{\beta} w_\infty = 0. \tag{2.35}$$

Corresponding to the vorticity (2.32), the far-field velocity fluctuation is

$$\boldsymbol{u}_\infty^{(c)} = \boldsymbol{u}_\infty \exp\{\mathrm{i}\hat{\alpha}_c(\bar{x} - \bar{t}) + \mathrm{i}\hat{\beta}_v \bar{y} + \mathrm{i}\hat{\beta}\bar{z}\}. \tag{2.36}$$

The solution for the entropy mode in the gust is given by

$$\hat{\tau}_c = \tau_\infty \mathrm{e}^{\mathrm{i}\hat{\beta}_e \bar{y}}, \quad \hat{\rho}_c = -\tau_\infty \mathrm{e}^{\mathrm{i}\hat{\beta}_e \bar{y}}, \tag{2.37}$$

where the constant τ_∞ is independent of Ω_∞. We have so far completed the specification of the disturbance in the free stream. Note that since $\hat{\alpha}_c = \hat{\omega}_c$, the resonant conditions (2.10) and (2.11) together with (2.28) give, to leading order,

$$\hat{\alpha}_{TS} = \frac{\hat{\omega}_s}{1 + M\cos\theta}, \quad \hat{\alpha}_c = \hat{\omega}_s. \tag{2.38}$$

The first relation above indicates that the frequency and directivity of the sound completely determine the wavenumber of the T–S wave that it can excite.

The $O(\epsilon^2 R^{3/16})$ terms in (2.16)–(2.19) represent the T–S wave, and they must be included so that the forced problem at the next order can have an acceptable solution. For our purpose, we only need p_{TS} and v_{TS}. They are governed by the equations

$$\frac{\partial^2 p_{TS}}{\partial \bar{y}^2} - \{(1 - M^2)\hat{\alpha}_{TS}^2 + \hat{\beta}^2\} p_{TS} = 0, \quad \frac{\partial v_{TS}}{\partial \bar{x}} = -\frac{\partial p_{TS}}{\partial \bar{y}}, \tag{2.39}$$

which have the solutions

$$p_{TS} = \hat{p}_1 A(x_1)\mathrm{e}^{-\hat{\gamma}_{TS}\bar{y}}, \quad v_{TS} = -\frac{\mathrm{i}\hat{\gamma}_{TS}}{\hat{\alpha}_{TS}}\hat{p}_1 A(x_1)\mathrm{e}^{-\hat{\gamma}_{TS}\bar{y}}, \tag{2.40}$$

with $\hat{\gamma}_{TS}^2 = (1 - M^2)\hat{\alpha}_{TS}^2 + \hat{\beta}^2$. In the supersonic regime, the condition

$$\hat{\beta}/\hat{\alpha}_{TS} > (M^2 - 1)^{1/2}$$

must be satisfied in order for the triple-deck approach to be applicable (Smith 1989). The function $A(x_1)$ is the amplitude of the T–S wave, the determination of which is the main purpose of the present paper.

The $O(\epsilon^2)$ terms are driven by the interaction between the convecting gust and the acoustic wave. Substituting (2.16)–(2.19) into (2.1)–(2.4), then at the quadratic order we obtain

$$\left(\frac{\partial}{\partial \bar{t}} + \frac{\partial}{\partial \bar{x}}\right)\rho_2 + \nabla \cdot \boldsymbol{u}_2 = -\left(\frac{\partial \rho_{TS}}{\partial x_1} + \frac{\partial u_{TS}}{\partial x_1}\right) - \nabla \cdot \left(\rho^{(s)}\boldsymbol{u}^{(c)} + \rho^{(c)}\boldsymbol{u}^{(s)}\right), \tag{2.41}$$

$$\left(\frac{\partial}{\partial \bar{t}} + \frac{\partial}{\partial \bar{x}}\right)\boldsymbol{u}_2 = -\nabla p_2 + \frac{\partial \boldsymbol{u}_{TS}}{\partial x_1} - \frac{\partial p_{TS}}{\partial x_1}\boldsymbol{i} + \rho^{(c)}\nabla p^{(s)} - (\boldsymbol{u}^{(s)} \cdot \nabla)\boldsymbol{u}^{(c)} - (\boldsymbol{u}^{(c)} \cdot \nabla)\boldsymbol{u}^{(s)}, \tag{2.42}$$

$$\left(\frac{\partial}{\partial \bar{t}} + \frac{\partial}{\partial \bar{x}}\right)\tau_2 - (\gamma - 1)M^2\left(\frac{\partial}{\partial \bar{t}} + \frac{\partial}{\partial \bar{x}}\right)p_2 + \frac{\partial \tau_{TS}}{\partial x_1} - (\gamma - 1)M^2\frac{\partial p_{TS}}{\partial x_1}$$
$$= -(\gamma - 1)M^2\left\{\rho^{(c)}\left(\frac{\partial}{\partial \bar{t}} + \frac{\partial}{\partial \bar{x}}\right)p^{(s)} - \boldsymbol{u}^{(c)} \cdot \nabla p^{(s)}\right\} - (\boldsymbol{u}^{(s)} \cdot \nabla)\tau^{(c)} - (\boldsymbol{u}^{(c)} \cdot \nabla)\tau^{(s)}, \tag{2.43}$$

$$\gamma M^2 p_2 = \tau_2 + \rho_2 + \rho^{(c)}\tau^{(s)} + \rho^{(s)}\tau^{(c)}. \tag{2.44}$$

Equations (2.42)–(2.44) can be reduced to a single equation for the pressure p_2

$$\left\{M^2\left(\frac{\partial}{\partial\bar{t}}+\frac{\partial}{\partial\bar{x}}\right)^2-\nabla^2\right\}p_2=2\mathrm{i}(1-M^2)\hat{\alpha}_{TS}A'(x_1)\hat{p}_1\,\mathrm{e}^{-\hat{\gamma}_{TS}\bar{y}}+R_{sv}+R_{se}, \tag{2.45}$$

where

$$R_{sv}=\nabla\cdot\left\{(\boldsymbol{u}^{(s)}\cdot\nabla)\boldsymbol{u}^{(c)}+(\boldsymbol{u}^{(c)}\cdot\nabla)\boldsymbol{u}^{(s)}\right\}+(\boldsymbol{u}^{(c)}\cdot\nabla)(\nabla\cdot\boldsymbol{u}^{(s)}), \tag{2.46}$$

$$R_{se}=\nabla\cdot\left(\tau^{(c)}\nabla p^{(a)}\right), \tag{2.47}$$

which are the forcing arising from the acoustic mode interacting with the vortical and entropy modes respectively. Each of them consists of the components proportional to the sum and difference frequencies, but only the latter component is relevant to the generation of T–S waves. Also since this component has a much lower frequency, the time derivative in (2.45) actually drops out with the result that (2.45) reduces to a Poisson equation when $M<1$ or an inhomogeneous wave equation when $M>1$. After a straightforward calculation aided by (2.35), we find that

$$R_{se}=-2p_a\tau_\infty\left\{(\hat{\alpha}_s^2+\hat{\beta}_s^2-\hat{\alpha}_s\hat{\alpha}_c)\cos(\hat{\beta}_s\bar{y})+\mathrm{i}\hat{\beta}_s\hat{\beta}_e\sin(\hat{\beta}_s\bar{y})\right\}\mathrm{e}^{\mathrm{i}\hat{\beta}_e\bar{y}}\,E, \tag{2.48}$$

$$R_{sv}=\left\{G_1\cos(\hat{\beta}_s\bar{y})+G_2\sin(\hat{\beta}_s\bar{y})\right\}\mathrm{e}^{\mathrm{i}\hat{\beta}_v\bar{y}}\,E+\left\{H_1\cos(\hat{\beta}_s\bar{y})+H_2\sin(\hat{\beta}_s\bar{y})\right\}\mathrm{e}^{-\hat{\gamma}\bar{y}}\,E, \tag{2.49}$$

where

$$\left.\begin{aligned}
G_1&=-2p_a^*M\left\{(\hat{\alpha}_s^2+\hat{\beta}_s^2-\hat{\alpha}_s\hat{\alpha}_c)\cos\theta\,u_\infty-\hat{\beta}_s\hat{\beta}_v\sin\theta\,v_\infty\right\},\\
G_2&=-2\mathrm{i}p_a^*M\left\{\hat{\beta}_s\hat{\beta}_v\cos\theta\,u_\infty-(\hat{\alpha}_s^2+\hat{\beta}_s^2-\hat{\alpha}_s\hat{\alpha}_c)\cos\theta\,v_\infty\right\},\\
H_1&=-2\mathrm{i}p_a^*\hat{\gamma}^{-1}M\left\{\hat{\alpha}_c(\hat{\alpha}_s^2+\hat{\beta}_s^2-\hat{\alpha}_s\hat{\alpha}_c)\cos\theta+\hat{\beta}_s(\hat{\alpha}_c^2+\hat{\beta}^2)\sin\theta\right\}v_\infty,\\
H_2&=-2\mathrm{i}p_a^*M(\hat{\alpha}_s^2+\hat{\beta}_s^2-2\hat{\alpha}_s\hat{\alpha}_c)\sin\theta\,v_\infty.
\end{aligned}\right\} \tag{2.50}$$

The solution for p_2 takes the form $p_2=(\hat{P}_2E+\text{c.c.})$, and

$$\begin{aligned}
\hat{P}_2=&\left\{\hat{p}_2+\frac{\mathrm{i}\hat{\alpha}_{TS}}{\hat{\gamma}_{TS}}(1-M^2)A'(x_1)\bar{y}\right\}\mathrm{e}^{-\hat{\gamma}_{TS}\bar{y}}+\left\{q_v^{(1)}\cos(\hat{\beta}_s\bar{y})+q_v^{(2)}\sin(\hat{\beta}_s\bar{y})\right\}\mathrm{e}^{\mathrm{i}\hat{\beta}_v\bar{y}}\\
&+\left\{q_e^{(1)}\cos(\hat{\beta}_s\bar{y})+q_e^{(2)}\sin(\hat{\beta}_s\bar{y})\right\}\mathrm{e}^{\mathrm{i}\hat{\beta}_e\bar{y}}+\left\{q_\gamma^{(1)}\cos(\hat{\beta}_s\bar{y})+q_\gamma^{(2)}\sin(\hat{\beta}_s\bar{y})\right\}\mathrm{e}^{-\hat{\gamma}\bar{y}},
\end{aligned}$$

where $\hat{p}_2$ is an undetermined function of x_1 representing the complementary solution, and

$$\left.\begin{aligned}
q_v^{(1)}&=\left[(\hat{\gamma}_{TS}^2+\hat{\beta}_s^2+\hat{\beta}_v^2)G_1+2\mathrm{i}\hat{\beta}_s\hat{\beta}_vG_2\right]/D_v,\\
q_v^{(2)}&=\left[-2\mathrm{i}\hat{\beta}_s\hat{\beta}_vG_1+(\hat{\gamma}_{TS}^2+\hat{\beta}_s^2+\hat{\beta}_v^2)G_2\right]/D_v,\\
q_e^{(1)}&=-2p_a^*\tau_\infty\left[(\hat{\gamma}_{TS}^2+\hat{\beta}_s^2+\hat{\beta}_e^2)(\hat{\alpha}_s^2+\hat{\beta}_s^2-\hat{\alpha}_s\hat{\alpha}_c)-2\hat{\beta}_s^2\hat{\beta}_e^2\right]D_e,\\
q_e^{(2)}&=2\mathrm{i}p_a^*\tau_\infty\left[2\hat{\beta}_s\hat{\beta}_e(\hat{\alpha}_s^2+\hat{\beta}_s^2-\hat{\alpha}_s\hat{\alpha}_c)-\hat{\beta}_s\hat{\beta}_e(\hat{\gamma}_{TS}^2+\hat{\beta}_s^2+\hat{\beta}_2^2)\right]/D_e,\\
q_\gamma^{(1)}&=\left[(\hat{\gamma}_{TS}^2+\hat{\beta}_s^2-\hat{\gamma}^2)H_1-2\hat{\beta}_s\hat{\gamma}H_2\right]/D_\gamma,\\
q_\gamma^{(2)}&=\left[2\hat{\beta}_s\hat{\gamma}H_1+(\hat{\gamma}_{TS}^2+\hat{\beta}_s^2-\hat{\gamma}^2)H_2\right]/D_\gamma,
\end{aligned}\right\} \tag{2.51}$$

with

$$D_v=(\hat{\gamma}_{TS}^2+\hat{\beta}_s^2+\hat{\beta}_v^2)^2-4\hat{\beta}_s^2\hat{\beta}_v^2. \tag{2.52}$$

The expressions for D_e and D_γ are the same as for D_v provided that $\hat{\beta}_v$ is replaced by $\hat{\beta}_e$ and $\mathrm{i}\hat{\gamma}$ respectively. Clearly as $\bar{y} \to 0$,

$$p_2 \to (\hat{p}_2 + F_p)E + \cdots, \quad \text{with} \quad F_p = q_e^{(1)} + q_v^{(1)} + q_\gamma^{(1)}. \tag{2.53}$$

By substituting p_2 into the vertical momentum equation in (2.42), it can be shown that

$$v_2 \to (\mathrm{i}\hat{\alpha}_{TS})^{-1}\left\{F_v - \frac{\mathrm{i}\hat{\alpha}_{TS}}{\hat{\gamma}_{TS}}(1-M^2)A'\hat{p}_1 + \hat{\gamma}_{TS}\hat{p}_2 + \frac{\mathrm{i}\hat{\gamma}_{TS}}{\hat{\alpha}_{TS}}A'\hat{p}_1\right\}E \quad \text{as} \quad \bar{y} \to 0, \tag{2.54}$$

where

$$F_v = -\left(\mathrm{i}\hat{\beta}_e q_e^{(1)} + \hat{\beta}_s q_e^{(2)}\right) - \left(\mathrm{i}\hat{\beta}_v q_v^{(1)} + \hat{\beta}_s q_v^{(2)}\right) - \left(-\hat{\gamma} q_\gamma^{(1)} + \hat{\beta}_s q_\gamma^{(2)}\right). \tag{2.55}$$

The forcing F_p and F_v due to the sound–gust interaction will be transmitted to the lower deck via the main deck. Since no further interaction takes place there, the components on the T–S wave scales arise merely as the response to the upper deck and satisfy the standard main-deck equations. The streamwise and vertical velocities have the familiar solutions (e.g. Smith 1989)

$$u = \epsilon^2 R^{5/16} BU'(\tilde{Y})E + \text{c.c.}, \quad v = -\epsilon^2 R^{-3/16}\frac{\partial}{\partial x}\{BU(\tilde{Y})E + \text{c.c.}\}, \tag{2.56}$$

where $\tilde{Y} = R^{1/2}y$ and $\partial/\partial x$ should be transformed according to (2.13). In order to match with the upper-deck solution, the displacement function B takes the form

$$B = A(x_1)B_1 + R^{-3/16}B_2(x_1), \tag{2.57}$$

with B_1 and B_2 being an undetermined constant and function respectively. By using (2.15) and (2.13), it can be shown that

$$u \to \epsilon^2 R^{5/16}\{\lambda_0 AB_1 + R^{-3/16}(\lambda_1 x_1 AB_1 + \lambda_0 B_2)\}E + \text{c.c.} \quad \text{as} \quad \tilde{Y} \to 0, \tag{2.58}$$

$$v \to -\epsilon^2 R^{3/16}\{\mathrm{i}\hat{\alpha}_{TS}AB_1 + R^{-3/16}(A'B_1 + \mathrm{i}\hat{\alpha}_{TS}B_2)\}E + \text{c.c.} \quad \text{as} \quad \tilde{Y} \to \infty. \tag{2.59}$$

3. The lower-deck response

In the lower deck, the flow is effectively incompressible and the appropriate transverse coordinate is defined by

$$Y = R^{5/8}y. \tag{3.1}$$

The mean flow may be approximated, to the required order, by $R^{-1/8}\lambda Y$, with the skin friction λ given by (2.15). The solution can be written as

$$u = R^{-1/8}(\lambda_0 + R^{-3/16}\lambda_1 x_1)Y + \epsilon U_s + \epsilon^2 R^{5/16}A(x_1)\tilde{U}_1 E + \epsilon^2 R^{1/8}\tilde{U}_2 E + \cdots, \tag{3.2}$$

$$v = \epsilon R^{-1/4}V_s + \epsilon^2 R^{1/16}A(x_1)\tilde{V}_1 E + \epsilon^2 R^{-1/8}\tilde{V}_2 E + \cdots, \tag{3.3}$$

$$w = \epsilon^2 R^{5/16}A(x_1)\tilde{W}_1 E + \epsilon^2 R^{1/8}\tilde{W}_2 E + \cdots, \tag{3.4}$$

$$p = \epsilon p_s + \epsilon^2 R^{3/16}A(x_1)\hat{p}_1 E + \epsilon^2 \tilde{P}_2 E + \cdots. \tag{3.5}$$

Here we have ignored the exponentially small signature of the convecting gust. The acoustic signature, represented by the $\tilde{U}_s$, $\tilde{V}_s$ and p_s, is not of our concern either since there is no interaction taking place in the lower deck. We concentrate on the T–S components. Substitution of these expansions together with (3.1) into (2.1)–(2.2)

yields the linearized boundary-layer equations (Smith 1989)

$$\mathrm{i}\hat{\alpha}_{TS}\tilde{U}_1 + \tilde{V}_{1,Y} + \mathrm{i}\hat{\beta}\tilde{W}_1 = 0, \tag{3.6}$$

$$\mathrm{i}(\hat{\alpha}_{TS}\lambda_0 Y - \hat{\omega}_{TS})\tilde{U}_1 + \lambda_0\tilde{V}_1 = -\mathrm{i}\hat{\alpha}_{TS}\hat{p}_1 + \tilde{U}_{1,YY}, \tag{3.7}$$

$$\mathrm{i}(\hat{\alpha}_{TS}\lambda_0 Y - \hat{\omega}_{TS})\tilde{W}_1 = -\mathrm{i}\hat{\beta}\hat{p}_1 + \tilde{W}_{1,YY}. \tag{3.8}$$

The above system is subject to the matching condition with the main deck:

$$\tilde{V}_{1,Y} \to -\mathrm{i}\hat{\alpha}_{TS}\lambda_0 B_1, \quad \tilde{W}_1 \to 0 \quad \text{as} \quad Y \to \infty, \tag{3.9}$$

and the no-slip condition $\tilde{U}_1 = \tilde{V}_1 = \tilde{W}_1 = 0$ on the wall ($Y = 0$); the latter leads to

$$\tilde{V}_{1,YYY}(0) = (\hat{\alpha}_{TS}^2 + \hat{\beta}^2)\hat{p}_1 \tag{3.10}$$

after setting $Y = 0$ in (3.7)–(3.8) and using (3.6). The constant B_1 in (3.9) is related to $\hat{p}_1$ via

$$\hat{\alpha}_{TS}^2 B_1 = \hat{\gamma}_{TS}\hat{p}_1, \tag{3.11}$$

a relation provided by matching the upper-deck solution (2.40) with the leading-order term in the main-deck solution (2.59).

By eliminating the pressure from (3.6)–(3.8), it can be shown that $\tilde{V}_{1,YY}$ satisfies

$$\left\{\frac{\partial^2}{\partial Y^2} - \mathrm{i}(\hat{\alpha}_{TS}\lambda_0 Y - \hat{\omega}_{TS})\right\}\tilde{V}_{1,YY} = 0, \tag{3.12}$$

which has the solution

$$\tilde{V}_{1,Y} = \int_{\eta_0}^{\eta} \mathrm{Ai}(\eta)\,\mathrm{d}\eta, \tag{3.13}$$

where Ai denotes the Airy function, and

$$\eta = (\mathrm{i}\hat{\alpha}_{TS}\lambda_0)^{1/3}Y + \eta_0, \quad \eta_0 = -\mathrm{i}\hat{\omega}_{TS}(\mathrm{i}\hat{\alpha}_{TS}\lambda_0)^{-2/3}\,. \tag{3.14}$$

Application of (3.9) and (3.10), together with (3.14) gives

$$\int_{\eta_0}^{\infty} \mathrm{Ai}(\zeta)\,\mathrm{d}\zeta = -\mathrm{i}\hat{\alpha}_{TS}\lambda_0 B_1, \quad (\mathrm{i}\hat{\alpha}_{TS}\lambda_0)^{2/3}\mathrm{Ai}'(\eta_0) = (\hat{\alpha}_{TS}^2 + \hat{\beta}^2)\hat{p}_1, \tag{3.15}$$

which with (3.11) lead to the dispersion relation (cf. Terent'ev 1981; Smith 1989)

$$\Delta(\lambda_0) = 0, \tag{3.16}$$

where

$$\Delta(\lambda_0) \equiv \mathrm{i}\hat{\alpha}_{TS}(\hat{\alpha}_{TS}^2 + \hat{\beta}^2)\int_{\eta_0}^{\infty}\mathrm{Ai}(\eta)\,\mathrm{d}\eta - \lambda_0\left[(1-M^2)\hat{\alpha}_{TS}^2 + \hat{\beta}^2\right]^{1/2}(\mathrm{i}\hat{\alpha}_{TS}\lambda_0)^{2/3}\mathrm{Ai}'(\eta_0). \tag{3.17}$$

The neutral wavenumber and frequency can be determined by

$$\hat{\alpha}_{TS} = \lambda_0^{5/4}\alpha_N, \quad \hat{\beta} = \lambda_0^{5/4}\beta_N, \quad \hat{\omega}_{TS} = \lambda_0^{3/2}\omega_N, \tag{3.18}$$

with α_N, β_N and ω_N given by

$$\alpha_N^{1/3}(\alpha_N^2 + \beta_N^2) = d_1\left((1-M^2)\alpha_N^2 + \beta_N^2\right)^{1/2}, \quad \omega_N = d_2\alpha_N^{2/3}, \tag{3.19}$$

where $d_1 \approx 1.001$ and $d_2 \approx 2.299$.

The terms $\tilde{U}_2$, $\tilde{V}_2$ etc. in (3.2)–(3.5) arise as the direct response to the forcing from

the upper deck. They are governed by the equations

$$\mathrm{i}\hat{\alpha}_{TS}\tilde{U}_2 + \tilde{V}_{2,Y} + \mathrm{i}\hat{\beta}\tilde{W}_2 = -A'(x_1)\tilde{U}_1, \tag{3.20}$$

$$\mathrm{i}(\hat{\alpha}_{TS}\lambda_0 Y - \hat{\omega}_{TS})\tilde{U}_2 + \lambda_0\tilde{V}_2 = -\mathrm{i}\hat{\alpha}_{TS}\tilde{P}_2 + \tilde{U}_{2,YY} - \Lambda(x_1)Y\tilde{U}_1 - \lambda_1 x_1\tilde{V}_1 - A'(x_1)\hat{p}_1, \tag{3.21}$$

$$\mathrm{i}(\hat{\alpha}_{TS}\lambda_0 Y - \hat{\omega}_{TS})\tilde{W}_2 = -\mathrm{i}\hat{\beta}\tilde{P}_2 + \tilde{W}_{2,YY} - \Lambda(x_1)Y\tilde{W}_1, \tag{3.22}$$

where Λ is defined by

$$\Lambda(x_1) = \lambda_0 A'(x_1) + \mathrm{i}\hat{\alpha}_{TS}\lambda_1 x_1 A. \tag{3.23}$$

These equations are coupled to the upper-deck Poisson equation (or inhomogeneous wave equation) via the matching conditions below. The boundary conditions again follow from the no-slip requirement on the wall and the matching with the main-deck solution (2.58), namely

$$\tilde{U}_2 = \tilde{V}_2 = \tilde{W}_2 = 0 \quad \text{at} \quad Y = 0\ ; \quad \tilde{U}_2 \to \lambda_0 B_2 + \lambda_1 x_1 A B_1, \quad \tilde{W}_2 \to 0 \quad \text{as} \quad Y \to \infty.$$

These in turn imply that

$$\tilde{V}_{2,Y} \to -\mathrm{i}\hat{\alpha}_{TS}\lambda_0 B_2 - \Lambda(x_1)B_1 \quad \text{as} \quad Y \to \infty, \tag{3.24}$$

$$\tilde{V}_{2,YYY} = (\hat{\alpha}_{TS}^2 + \hat{\beta}^2)(\hat{p}_2 + F_p) - 2\mathrm{i}\hat{\alpha}_{TS}A'\hat{p}_1 \quad \text{at} \quad Y = 0. \tag{3.25}$$

Here we have used the result that $\tilde{P}_2 = \hat{p}_2 + F_p$. The matching between the upper-deck solution(2.54) and the second term in the main-deck solution (2.59) shows that

$$\hat{\alpha}_{TS}^2 B_2 - 2\mathrm{i}\hat{\alpha}_{TS}A'(x_1)B_1 = \hat{\gamma}_{TS}\hat{p}_2 - \frac{\mathrm{i}\hat{\alpha}_{TS}}{\hat{\gamma}_{TS}}(1 - M^2)A'(x_1)\hat{p}_1 + F_v. \tag{3.26}$$

Now eliminating the pressure from (3.20)–(3.22), we can show that $\tilde{V}_{2,YY}$ satisfies

$$\left\{\frac{\partial^2}{\partial Y^2} - \mathrm{i}(\hat{\alpha}_{TS}\lambda_0 Y - \hat{\omega}_{TS})\right\}\tilde{V}_{2,YY} = \Lambda(x_1)Y\tilde{V}_{1,YY} = \Lambda(x_1)(\eta - \eta_0)\mathrm{Ai}(\eta). \tag{3.27}$$

The terms F_p and F_v in (3.25) and (3.26) represent the forcing, which is transmitted to the lower deck through the matching. In order for equation (3.27) to have a solution which also satisfies the boundary conditions (3.24) and (3.25), a solvability condition must be satisfied. This could be derived by following the procedure given by Smith (1979*b*) for the weakly nonlinear instability. Alternatively one may write out, via order reduction, the general solution of (3.27) in terms of an Airy function, and then obtain the solvability condition by applying the boundary conditions. We shall take the latter course since for the present problem the right-hand side of (3.27) is so simple that the general solution is found to be

$$\tilde{V}_{2,Y} = \tfrac{1}{3}(\mathrm{i}\hat{\alpha}_{TS}\lambda_0)^{-1}\Lambda(x_1)\{(\eta - 3\eta_0)\mathrm{Ai}(\eta) + 2\eta_0\mathrm{Ai}(\eta_0)\} + q_2\int_{\eta_0}^{\eta}\mathrm{Ai}(\eta)\,\mathrm{d}\eta. \tag{3.28}$$

The boundary conditions (3.24) and (3.25) leads to

$$\tfrac{2}{3}(\mathrm{i}\hat{\alpha}_{TS}\lambda_0)^{-1}\Lambda\eta_0\mathrm{Ai}(\eta_0) + q_2\int_{\eta_0}^{\infty}\mathrm{Ai}(\eta)\,\mathrm{d}\eta = -\mathrm{i}\hat{\alpha}_{TS}\lambda_0 B_2 - \Lambda B_1, \tag{3.29}$$

$$\tfrac{2}{3}(\mathrm{i}\hat{\alpha}_{TS}\lambda_0)^{-1/3}\Lambda\{\mathrm{Ai}'(\eta_0) - \eta_0\mathrm{Ai}''(\eta_0)\} + (\mathrm{i}\hat{\alpha}_{TS}\lambda_0)^{2/3}q_2\mathrm{Ai}'(\eta_0) = (\hat{\alpha}_{TS}^2 + \hat{\beta}^2)(\hat{p}_2 + F_p) - 2\mathrm{i}\hat{\alpha}_{TS}A'\hat{p}_1. \tag{3.30}$$

Eliminating B_2 and $\hat{p}_2$ from (3.26), (3.29)–(3.30), and using (3.15), we obtain

$$aA' + b(\mathrm{i}\hat{\alpha}_{TS}\lambda_1 x_1/\lambda_0)A + (\hat{\alpha}_{TS}^2 + \hat{\beta}^2)^{-1}\Delta(\lambda_0)q_2 = -\lambda_0(\hat{\gamma}_{TS}F_p - F_v)\,, \tag{3.31}$$

where

$$a = \tfrac{2}{3}\eta_0\mathrm{Ai}(\eta_0) + \left(\frac{\hat{\beta}^2}{\hat{\gamma}_{TS}^2} + \frac{2\hat{\alpha}_{TS}^2}{\hat{\alpha}_{TS}^2 + \hat{\beta}^2}\right)\int_{\eta_0}^{\infty}\mathrm{Ai}(\eta)\,\mathrm{d}\eta$$
$$+\frac{2}{3}\frac{\hat{\gamma}_{TS}(\mathrm{i}\hat{\alpha}_{TS}\lambda_0)^{5/3}}{\hat{\alpha}_{TS}^2(\hat{\alpha}_{TS}^2 + \hat{\beta}^2)}\{\mathrm{Ai}'(\eta_0) - \eta_0\mathrm{Ai}''(\eta_0)\},$$

$$b = \tfrac{2}{3}\eta_0\mathrm{Ai}(\eta_0) - \int_{\eta_0}^{\infty}\mathrm{Ai}(\eta)\,\mathrm{d}\eta + \frac{2}{3}\frac{\hat{\gamma}_{TS}(\mathrm{i}\hat{\alpha}_{TS}\lambda_0)^{5/3}}{\hat{\alpha}_{TS}^2(\hat{\alpha}_{TS}^2 + \hat{\beta}^2)}\{\mathrm{Ai}'(\eta_0) - \eta_0\mathrm{Ai}''(\eta_0)\}.$$

Since $\Delta(\lambda_0) = 0$ (see (3.16)), equation (3.31) further reduces to

$$A'(x_1) = \sigma x_1 A + N \tag{3.32}$$

with σ and N given by

$$\sigma = -\mathrm{i}\hat{\alpha}_{TS}\lambda_1 b/(a\lambda_0), \quad N = -\lambda_0(\hat{\gamma}_{TS}F_p - F_v)/a. \tag{3.33}$$

4. Matching with the upstream response and coupling coefficient

On assuming that the amplitude of the T–S wave vanishes as $x_1 \to -\infty$, the amplitude equation (3.32) has the solution

$$A(x_1) = N\,\mathrm{e}^{\sigma x_1^2/2}\int_{-\infty}^{x_1}\mathrm{e}^{-\sigma\xi^2/2}\,\mathrm{d}\xi. \tag{4.1}$$

More precisely, it can be shown that as $x_1 \to -\infty$,

$$A(x_1) \to (N/\sigma)(-x_1)^{-1} + O(x_1)^{-3}. \tag{4.2}$$

That the above behaviour of $A(x_1)$ implies the matching with the upstream forced response can be seen as follows. At an upstream location, x say, the forced solution in the lower deck has expansions similar to (3.2)–(3.5) provided that the T–S wave terms and the mean-flow deviation are dropped. The solution of the forced response with the difference wavenumber $(\hat{\alpha}_c - \hat{\alpha}_s)$ then can be found in a similar way as for $\tilde{U}_2$ and $\tilde{V}_2$. In fact, one arrives at the same equation as (3.31) except that $A = 0$ and λ_0 is replaced by λ. We can identify q_2 as the amplitude of the forced response, A_F. Since $\Delta(\lambda) \neq 0$,

$$A_F \equiv q_2 = -\frac{\lambda(\hat{\alpha}_{TS}^2 + \hat{\beta}^2)}{\Delta(\lambda)}(\hat{\gamma}_{TS}F_p - F_v).$$

A Taylor expansion of $\Delta(\lambda)$ about λ_0 shows that as $x \to x_0$,

$$A_F \to \frac{\mathrm{i}\lambda_0^2(\hat{\gamma}_{TS}F_p - F_v)}{\hat{\alpha}_{TS}b(\lambda - \lambda_0)}. \tag{4.3}$$

The right-hand side is exactly $R^{3/16}(N/\sigma)(-x_1)^{-1}$ after substituting in (2.15) and (3.33). Therefore (4.2) and (4.3) imply that

$$A(x_1) \to R^{-3/16}A_F \quad \text{as} \quad x_1 \to -\infty,$$

which is precisely what is required for the matching of the velocities in the two stages.

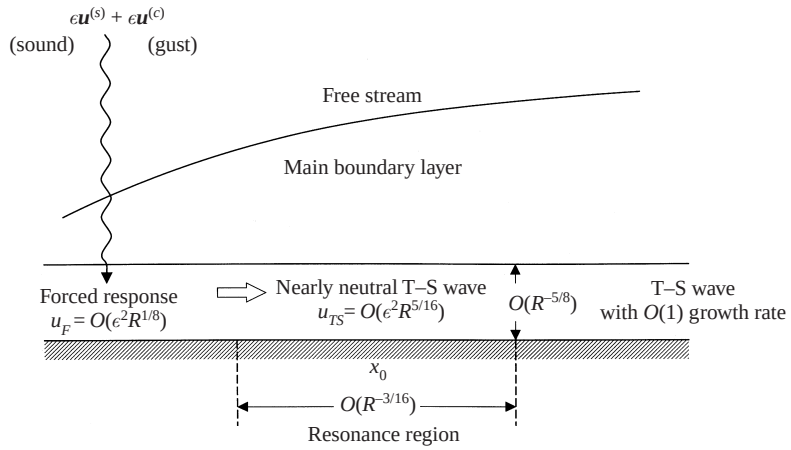

FIGURE 1. Sketch of the receptivity process due to the acoustic–gust interaction.

We now turn to the downstream limit, $x_1 \to +\infty$. In this limit,

$$A(x_1) \to A_\infty \, \mathrm{e}^{\sigma x_1^2/2}, \quad \text{with} \quad A_\infty = N \int_{-\infty}^{\infty} \mathrm{e}^{-\sigma \xi^2/2} \, \mathrm{d}\xi. \tag{4.4}$$

As $x_1 = O(R^{3/16})$, the T–S wave eventually acquires an $O(1)$ growth rate, and evolves exponentially over the fast streamwise scale $\bar{x}$. The amplitude now takes the usual WKBJ form

$$A \, \mathrm{e}^{\mathrm{i}\hat{\alpha}_{TS}\bar{x}} = A_\infty \exp\left\{ \mathrm{i}R^{3/8} \int_{x_0}^{x} \hat{\alpha}_{TS}(x) \, \mathrm{d}x \right\} \tag{4.5}$$

with the complex wavenumber $\hat{\alpha}_{TS}(x)$ being determined by local parallel stability theory. Clearly the constant A_∞ appears as the (scaled) initial amplitude of this subsequent stage. Note that the non-parallelism has been crucial for ensuring the matching of the solution in the vicinity of the neutral point with those upstream and downstream.

Taking the above results together, we may summarize the receptivity process as follows. The convecting gust and an acoustic wave with wavenumbers $\hat{\alpha}_c$ and $\hat{\alpha}_s$ respectively interact in the free stream, generating an $O(\epsilon^2)$ forcing, which then drives a forced solution with $O(\epsilon^2 R^{1/8})$ streamwise velocity within the boundary layer. As the flow evolves through the neutral position of a T–S wave with the wavenumber $(\hat{\alpha}_c - \hat{\alpha}_s)$, the forcing at the difference wavenumber (frequency) becomes in resonance with this T–S wave and the non-parallel-flow effect comes into play. As a result of these, the T–S wave develops from the forced solution and acquires an amplitude of $O(\epsilon^2 R^{5/16})$. The T–S wave so generated continues to grow and finally enters the order-one growth-rate stage. The whole process is illustrated schematically in figure 1.

In order to be precise, we shall use the maximum value of the streamwise velocity component of the T–S waves as an indicator of their magnitude, since that is the quantity that can be most accurately measured experimentally. First it can be shown by using (3.8), (3.15) and (3.14) that

$$\tilde{W}_1 = \frac{\mathrm{i}\hat{\beta}\mathrm{Ai}'(\eta_0)}{\hat{\alpha}_{TS}^2 + \hat{\beta}^2} Ł(\eta), \tag{4.6}$$

where $Ł(\eta)$ is the solution to the equation $Ł'' - \eta Ł = 1$ satisfying boundary condition

$L(\eta_0) = 0$ and $L(\infty) = 0$. It then follows from (3.2), (3.6), (3.13) and (4.6) that the maximum magnitude of the streamwise velocity at the neutral point is given by

$$u_{TS} = \epsilon^2 R^{5/16} \hat{\alpha}_{TS}^{-1} A_\infty U_m, \tag{4.7}$$

where

$$U_m = \max_\eta \left| \int_{\eta_0}^{\eta} \mathrm{Ai}(\eta)\, \mathrm{d}\eta - \frac{\beta_N^2}{\alpha_N^2 + \beta_N^2} \mathrm{Ai}'(\eta_0) Ł(\eta) \right|. \tag{4.8}$$

While u_{TS} is an appropriate measure of receptivity, it can hardly be measured directly in experiments. Instead one usually has to measure the streamwise velocity of the T–S wave at some disturbance downstream of the neutral point. That velocity is then extrapolated back to the neutral point in order to make a comparison with u_{TS} defined by (4.7).

The quantity A_∞ consists of two parts, $A_\infty^{(v)}$ and $A_\infty^{(e)}$, which are contributed by the sound-vorticity and sound-entropy interactions respectively; see (2.45) and (2.46)–(2.47). We define the respective *coupling coefficients*, C_V and C_E, for the vortical and entropy modes, as follows:

$$C_V = \epsilon^2 R^{5/16} \hat{\alpha}_{TS}^{-1} A_\infty^{(v)} U_m / (\epsilon u_\infty p_a), \quad C_E = \epsilon^2 R^{5/16} \hat{\alpha}_{TS}^{-1} A_\infty^{(e)} U_m / (\epsilon \tau_\infty p_a). \tag{4.9}$$

While the scalings adopted in our analysis are convenient for theoretical purposes, in experiments it is customary to scale the dimensional frequencies of the acoustic disturbance and the T–S wave, ω_s^* and ω_{TS}^*, as

$$f_s = \omega_s^* \nu_\infty / U_\infty^2, \quad f_{TS} = \omega_{TS}^* \nu_\infty / U_\infty^2.$$

Correspondingly, the dimensional wavenumbers of the sound, the gust and the T–S wave, α_s^*, α_c^*, α_{TS}^* and β^* are non-dimensionalized by U_∞/ν_∞, giving $\tilde{\alpha}_s = \alpha_s^* \nu_\infty / U_\infty$, etc. In terms of f_s, we have

$$\tilde{\alpha}_s = \frac{M \cos\theta}{1 + M \cos\theta} f_s, \quad \tilde{\alpha}_c = f_s, \tag{4.10}$$

$$\tilde{\alpha}_{TS} = \frac{f_s}{1 + M \cos\theta}.$$

Introducing the rescaling in (2.8), (3.18)–(3.19) and using (2.14), we find from these relations that the location of the neutral position, non-dimensionalized by ν_∞ / U_∞, is given by

$$\tilde{x}_0 \equiv U_\infty x_0^* / \nu_\infty = \chi^2 \left\{ \frac{f_s}{\alpha_N (1 + M \cos\theta)} \right\}^{-8/5}, \tag{4.11}$$

and that

$$\tilde{\beta} = \frac{\beta_N}{\alpha_N (1 + M \cos\theta)} f_s, \tag{4.12}$$

$$f_{TS} = \left\{ \frac{f_s}{\alpha_N (1 + M \cos\theta)} \right\}^{6/5} \omega_N. \tag{4.13}$$

A simple correspondence exists between $\hat{\alpha}_s$ and $\tilde{\alpha}_s$ etc., using which along with (4.10) and (4.12) in (2.50)–(2.55) indicates that $(\hat{\gamma}_{TS} F_p - F_v)/\hat{\alpha}_{TS}$ is independent of f_s. The streamwise length scale l can be taken as x_0^* so that $x_0 = 1$. It then follows from (3.33) and (4.4), and (4.8) that $\hat{\alpha}_{TS}^{-1} A_\infty$ and U_m are independent of f_s. Now since the

Reynolds number R is actually $\tilde{x}_0$ defined by (4.11), equation (4.9) implies that C_V and C_E scale with the sound frequency f_s as follows:

$$C_V = \epsilon\kappa_v f_s^{-1/2}, \quad C_E = \epsilon\kappa_e f_s^{-1/2}, \tag{4.14}$$

where κ_v (κ_e) depends on M, θ, β_N, v_∞/u_∞ and β_v (β_e) with $\beta_v = \tilde{\beta}_v/f_s$ and $\beta_e = \tilde{\beta}_e/f_s$. The above relations indicate that the low-frequency components in the acoustic disturbance are more efficient in exciting T–S waves. It should be noted, however, that a large coupling coefficient does not necessarily imply a large magnitude of the generated T–S wave, because the latter depends also on the amplitude of the relevant component in the gust, i.e. on the spectra of the gust. The sizes of the coupling coefficients and the T–S wave amplitude for typical parameter values will be estimated in § 6.

5. Statistics of T–S waves generated by isotropic turbulence

Obviously a gust consisting of a single Fourier mode is a highly idealized model, and can be of relevance only when a particular component is introduced artificially by some means so as to dominate the naturally occurring ones. In reality, the turbulence in the free stream consists of components of different frequencies and wavenumbers, and thus can be better represented by the integral over all Fourier modes (cf. (2.32) and (2.36))

$$\begin{Bmatrix} \boldsymbol{u}_\infty^{(c)} \\ \tau_\infty^{(c)} \end{Bmatrix} = \int_{-\infty}^{\infty} \begin{Bmatrix} \boldsymbol{u}_\infty(\boldsymbol{k}) \\ \tau_\infty(\boldsymbol{k}) \end{Bmatrix} \mathrm{e}^{\mathrm{i}(\boldsymbol{k}\cdot\tilde{\boldsymbol{x}} - k_1\tilde{t})}\,\mathrm{d}\boldsymbol{k}, \tag{5.1}$$

where $\boldsymbol{k} = (\tilde{\alpha}_c, \tilde{\beta}_v, \tilde{\beta})$ and $\tilde{\boldsymbol{x}} = (\tilde{x}, \tilde{y}, \tilde{z})$, non-dimensionalized by U_∞/v_∞ and v_∞/U_∞ respectively, and $\tilde{t}$ is normalized by v_∞/U_∞^2. For brevity, we shall omit the tilde over $\boldsymbol{x}$ and t throughout this section. As in many studies of turbulence undergoing rapid distortion (e.g. Hunt 1973; Hunt & Graham 1978; Goldstein 1978, 1979), the free-stream turbulence is assumed to be statistically stationary and homogeneous, and that the spectra of the velocity and the temperature (scalar) fluctuations, $\Phi_{ij}^{(\infty)}$ and $\Phi_s^{(\infty)}$ say, are known. The spectrum of a random velocity field $\boldsymbol{u} = (u_1, u_2, u_3)$ is defined as the Fourier transform of the velocity covariance (correlation) tensor (Batchelor 1953)

$$R_{ij}(\boldsymbol{x}, \boldsymbol{r}, \tau) = \overline{u_i(\boldsymbol{x}, t)u_j(\boldsymbol{x} + \boldsymbol{r}, t + \tau)}, \tag{5.2}$$

that is

$$\Phi_{ij}(\boldsymbol{k}; \boldsymbol{x}) = \frac{1}{(2\pi)^3} \int_{-\infty}^{\infty} R_{ij}(\boldsymbol{x}, \boldsymbol{r}, 0)\,\mathrm{e}^{-\mathrm{i}\boldsymbol{k}\cdot\boldsymbol{r}}\,\mathrm{d}\boldsymbol{r}. \tag{5.3}$$

Likewise, the spectrum of a temperature fluctuation, $\Phi_s^{(\infty)}$, is defined as the Fourier transform of the temperature covariance.

The acoustic field is also random in reality. However, in order to make further progress, we make the assumption that the sound is deterministic. This is completely justified for the laboratory situation as the sound can be introduced in a well-controlled manner. The random nature of the gust renders the direct measurement of κ_v and κ_e impossible. Instead, we need to consider the statistical properties of the T–S waves. A natural quantity to compute is the spectrum tensor of the T–S waves, from which one may then calculate the mean-square value of the streamwise velocity fluctuation in the T–S waves. To this end, we observe that for each T–S wave, its

streamwise velocity at a downstream location, $\tilde{x}$ say, can be written as

$$u_{TS} = \epsilon^2 f_s^{-1/2} p_a \{(a_{11}u_\infty + a_{12}v_\infty) + b_1\tau_\infty\} \exp\left\{\mathrm{i}\int_{\tilde{x}_0}^{\tilde{x}} \tilde{\alpha}_{TS}(\tilde{x})\,\mathrm{d}\tilde{x}\right\} \tag{5.4}$$

by using (4.7), (4.5), (4.4) and (3.33), and substituting in the expressions for F_p and F_v. The constants a_{11}, a_{12} and b_1 can be obtained explicitly, but for brevity we omit their expressions. Similar results hold for other velocity components and the temperature. Due to the linear relation between u_{TS} and u_∞, v_∞ and τ_∞, the relation between the T–S spectrum, Φ_{ij}, and the free-stream spectra, $\Phi_{ij}^{(\infty)}$ and $\Phi_s^{(\infty)}$ can be established, and are the same as those given by Hunt (1973) despite the T–S waves not being involved there. In particular, the component Φ_{11}, which is of our prime interest, is

$$\Phi_{11}^{(v)} = \epsilon^4 p_a^2 f_s^{-1}\left\{\int_{-\infty}^{\infty} a_{1k}^* a_{1l}\,\Phi_{kl}^{(\infty)}\,\mathrm{d}\tilde{\beta}_v\right\} \mathrm{e}^{2\tilde{N}}, \tag{5.5}$$

$$\Phi_{11}^{(e)} = \epsilon^4 p_a^2 f_s^{-1}\left\{\int_{-\infty}^{\infty} |b_1|^2\,\Phi_s^{(\infty)}\,\mathrm{d}\tilde{\beta}_v\right\} \mathrm{e}^{2\tilde{N}}, \tag{5.6}$$

where $\Phi_{11}^{(v)}$ and $\Phi_{11}^{(e)}$ denote the spectra of the T–S waves generated by the vorticity and entropy fluctuations respectively (and are normalized by $U_\infty(v_\infty/U_\infty)^3$), and

$$\tilde{N}(\tilde{\beta}, \tilde{x}) = -\int_{\tilde{x}_0}^{\tilde{x}} \mathrm{Im}\big(\tilde{\alpha}_{TS}(\tilde{x})\big)\,\mathrm{d}\tilde{x}$$

is the N-factor. Here we are able to consider the spectra of the T–S waves generated by the vorticity and entropy fluctuations separately on the assumption that there is no cross-correlation between the two types of fluctuations. Such an assumption, which is not unreasonable in view of the independent nature of these two types of motions, is also needed in other applications (e.g. Goldstein 1979).

For simplicity, we assume that the free-stream turbulence is isotropic, for which the spectrum tensor has the following representation (Batchelor 1953):

$$\Phi_{ij}^{(\infty)} = \frac{E(k)}{4\pi k^4}\big(k^2\delta_{ij} - k_i k_j\big), \tag{5.7}$$

where $k = |\boldsymbol{k}|$ and $E(k)$ is the energy spectrum function (normalized by $U_\infty^2(v_\infty/U_\infty)$), and is related to the longitudinal one-dimensional spectrum function $E_1(k)$ via

$$E(k) = k^3 \frac{\mathrm{d}}{\mathrm{d}k}\left(\frac{1}{k}\frac{\mathrm{d}}{\mathrm{d}k}E_1(k)\right). \tag{5.8}$$

An often used $E_1(k)$ is the von Kármán spectrum (Hinze 1959)

$$E_1(k) = 2a_0\overline{u^2}_\infty R_\Lambda\big\{1 + (R_\Lambda k)^2\big\}^{-5/6}, \quad \text{with} \quad a_0 = \frac{\sqrt{\pi}\,\Gamma(\frac{5}{6})}{\Gamma(\frac{1}{3})}, \tag{5.9}$$

where $\epsilon(\overline{u^2}_\infty)^{1/2}$ is the root mean square of the streamwise velocity of the free-stream fluctuation, and

$$R_\Lambda = a_0 U_\infty \Lambda_e / v_\infty$$

with Λ_e being the integral length of the turbulence. We note that there are other choices available for $E_1(k)$ (e.g. Gulyaev *et al.* 1989). Inserting (5.8 and (5.9) into (5.7), we obtain

$$\Phi_{ij}^{(\infty)}(\boldsymbol{k}) = \frac{55}{9}\frac{\overline{u^2}_\infty}{2\pi^2} a_0 R_\Lambda^5 \big(1 + (R_\Lambda k)^2\big)^{-17/6}\big(k^2\delta_{ij} - k_i k_j\big). \tag{5.10}$$

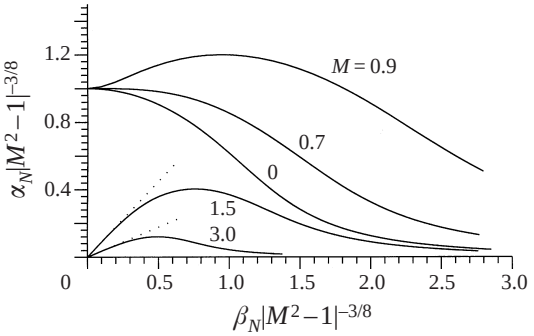

FIGURE 2. Neutral modes of T–S waves at different Mach numbers. The dotted lines represent the small-β_N asymptote: $\beta_N/\alpha_N = (M^2-1)^{1/2}$ (Smith 1989).

The spectrum of the temperature fluctuation is chosen to be (see (3-182) and (3-221) in Hinze 1959)

$$\Phi_s^{(\infty)}(k) = \frac{10}{3}\frac{\overline{\tau^2}_\infty}{(2\pi)^2} a_0 R_\Lambda^3 \left(1 + (R_\Lambda k)^2\right)^{-11/6}. \tag{5.11}$$

The calculation of the spectra $\Phi_{11}^{(v)}$ and $\Phi_{11}^{(e)}$ at a fixed point downstream involves computing the integral growth rate (or rather the N-factor). This is a rather separate computation and is well-documented elsewhere. We choose to avoid repeating this by dropping the exponential factors in (5.5) and (5.6). The resulting expressions naturally measure the efficiency of various components in the gust in generating the T–S waves, and so we shall still refer to them as 'spectra'. Unlike κ_v (or κ_e), they have taken into account the respective amplitude of each component in the free-stream turbulence.

6. Parametric study and discussion of the results

6.1. *Results for a single component*

In order to gain further quantitative information about the efficiency of the receptivity, the dependence of κ_v and κ_e on the parameters is investigated. This involves solving the dispersion relation (3.16) and calculating the functions $\mathrm{Ai}(\eta)$ and $Ł(\eta)$ in (4.8) numerically. These were done using the Newton–Raphson iteration and a fourth-order Runge–Kutta method respectively. Figure 2 shows α_N (the scaled streamwise wavenumber) as a function of β_N (the scaled spanwise wavenumber) for different Mach numbers. Note that in the subsonic regime, α_N tends to a finite value as $\beta_N \to 0$. However, in the supersonic regime α_N tends to zero also, but the ratio $\beta_N/\alpha_N \to (M^2-1)^{1/2}$ as shown by Smith (1989). It turns out that κ_v and κ_e exhibit somewhat different features in subsonic and supersonic regimes. So the results for each regime will be presented separately. The ratio v_∞/u_∞ is taken to be unity.

The case $M = 0.5$ is chosen as a representative for the subsonic regime. In figure 3, we show the contours of κ_v on the (β_v, β_N)-plane for different incident angles of the sound. For θ close to zero, κ_v attains its maximum at $\beta_N = 0$ implying that the sound–vorticity interaction favours the excitation of planar (or a band of nearly planar) T–S waves when the incident sound wave propagates along the free stream. But as θ increases, the maximum shifts to a finite β_N, and when θ is close to $\pi/2$, the maximum is attained at the large-β_N end. This implies that when a sound wave

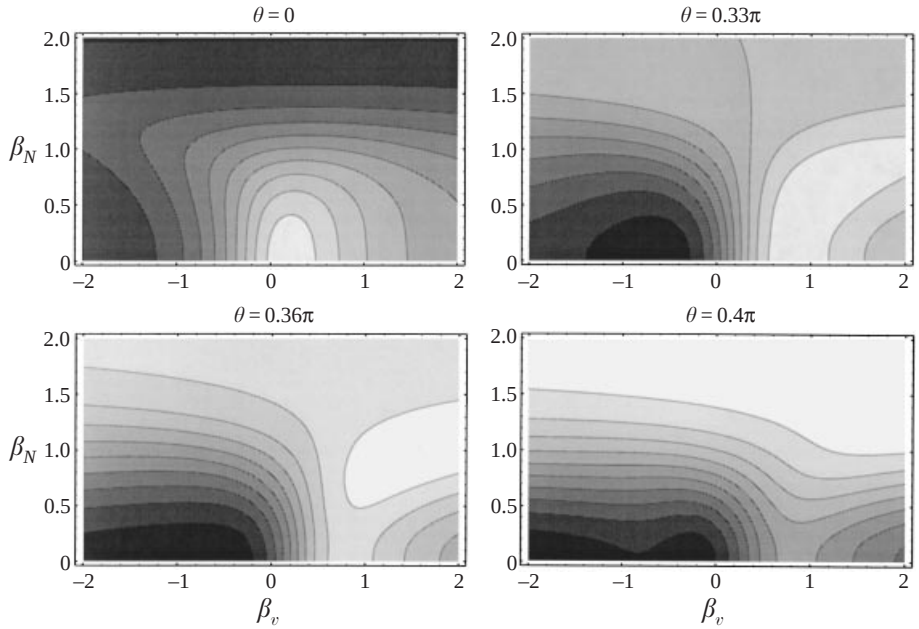

FIGURE 3. Contours of κ_v at different θ values ($M = 0.5$). (In all the contour plots, the contour value decreases with the grey degree.)

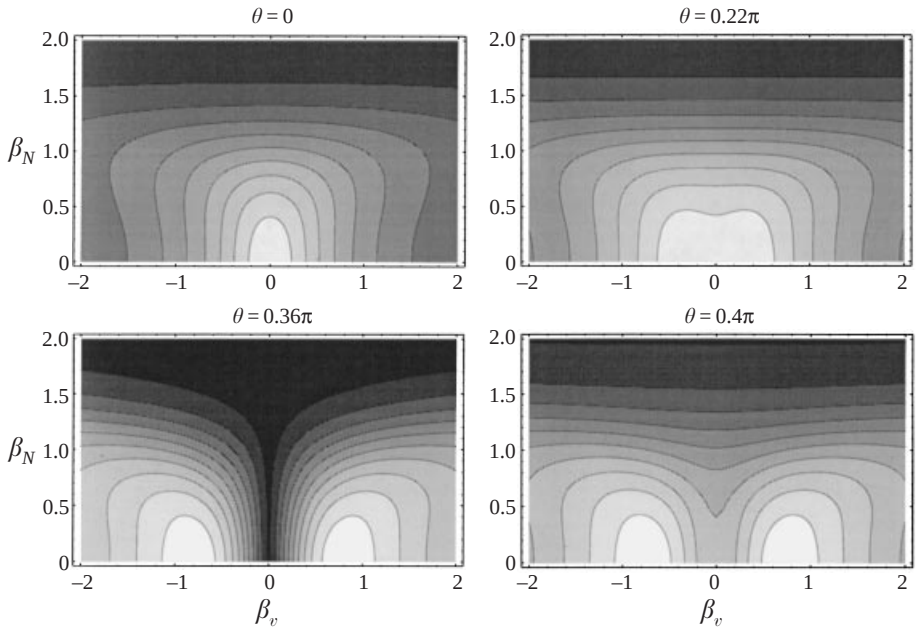

FIGURE 4. Contours of κ_e at different θ values ($M = 0.5$).

impinges perpendicular to the wall, the acoustic–vorticity interaction is most efficient in exciting a band of highly oblique T–S waves. In contrast, the sound–entropy interaction always tends to excite planar T–S waves, as is shown by contours in figure 4. The above features can be seen more clearly in figure 5(a, b), which illustrates how

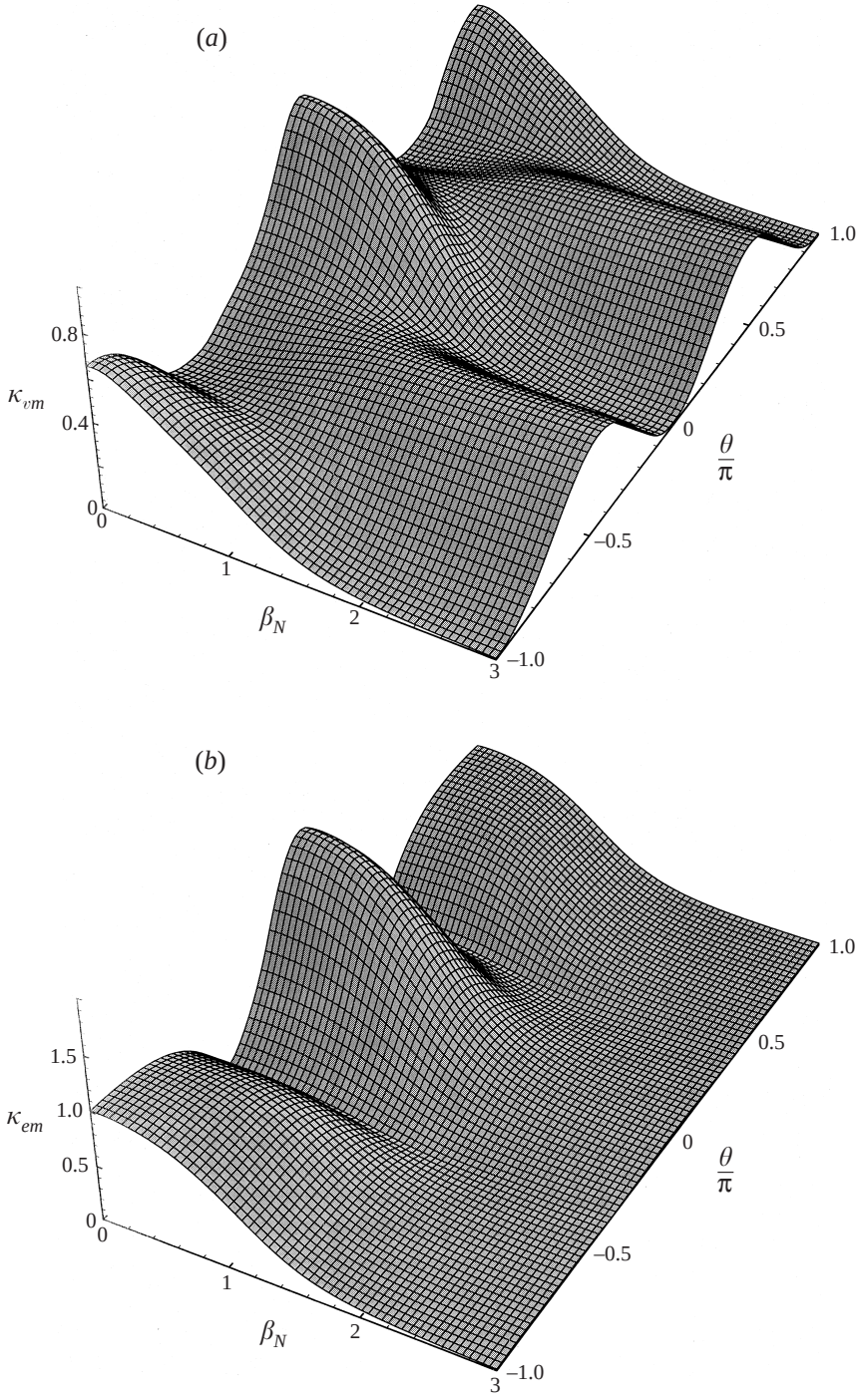

FIGURE 5. Variation of (*a*) κ_{vm} and (*b*) κ_{em} with respect to θ and β_N. $M = 0.5$.

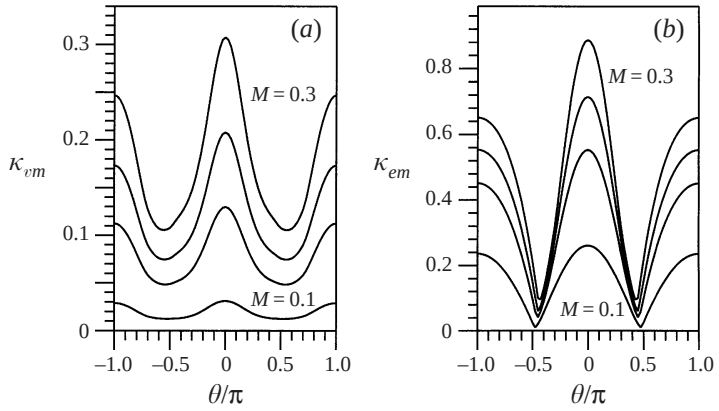

FIGURE 6. Receptivity for planar T–S waves at different Mach numbers ($M = 0.1$, 0.2, 0.25, 0.3). (a) κ_{vm} and (b) κ_{em} vs. θ.

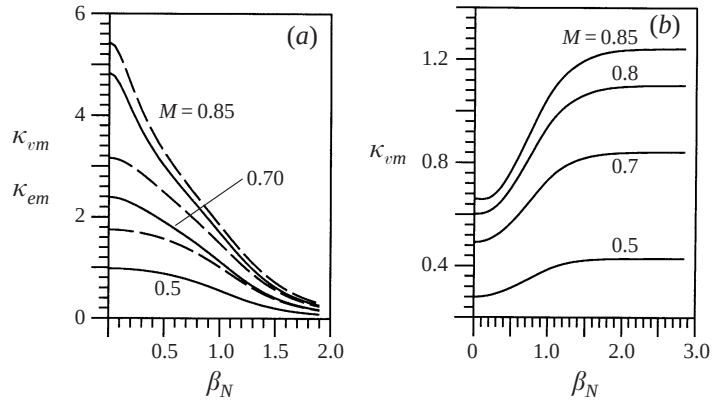

FIGURE 7. (a) κ_{vm} (solid line) and κ_{em} (dashed line) vs. β_N for parallel incident sound ($\theta = 0$). (b) κ_{vm} vs. β_N for perpendicular incident sound ($\theta = \pi/2$). $M = 0.5$, 0.7, 0.8, 0.85.

κ_{vm} and κ_{em} vary with respect to θ and β_N, where

$$\kappa_{vm} \equiv \max_{\beta_v} \kappa_v(\beta_v, \beta_N; M, \theta), \quad \kappa_{em} \equiv \max_{\beta_e} \kappa_v(\beta_e, \beta_N; M, \theta).$$

The generation of planar T–S waves is of particular relevance for $M < 0.5$ since in this range of Mach numbers, they are more unstable than their three-dimensional counterparts (Smith 1989). In figure 6(a, b), we plot κ_{vm} and κ_{em} (with $\beta_N = 0$) against θ for different Mach numbers. It is noted that they have peaks at $\theta = 0$ and π, with the value at $\theta = 0$ being only slightly larger than that at $\theta = \pi$, This means that as far as the excitation of the planar T–S waves is concerned, upstream and downstream propagating acoustic waves are almost equally efficient. Admittedly the coupling is weak for very small Mach numbers. But it becomes stronger rather quickly as M increases. For example, κ_{vm} and κ_{em} vary from 0.03 and 0.26 to 0.97 and 1.75 respectively as M is raized from 0.1 to 0.5.

For $0.5 < M < 1$, oblique T–S waves become more unstable (Smith 1989) and so the generation of these waves cannot be ignored and probably becomes more important. The characteristics of κ_{vm} and κ_{em} are similar to figure 5, except that the peak at $\theta = \pi$ becomes progressively milder (compared with the main one at $\theta = 0$)

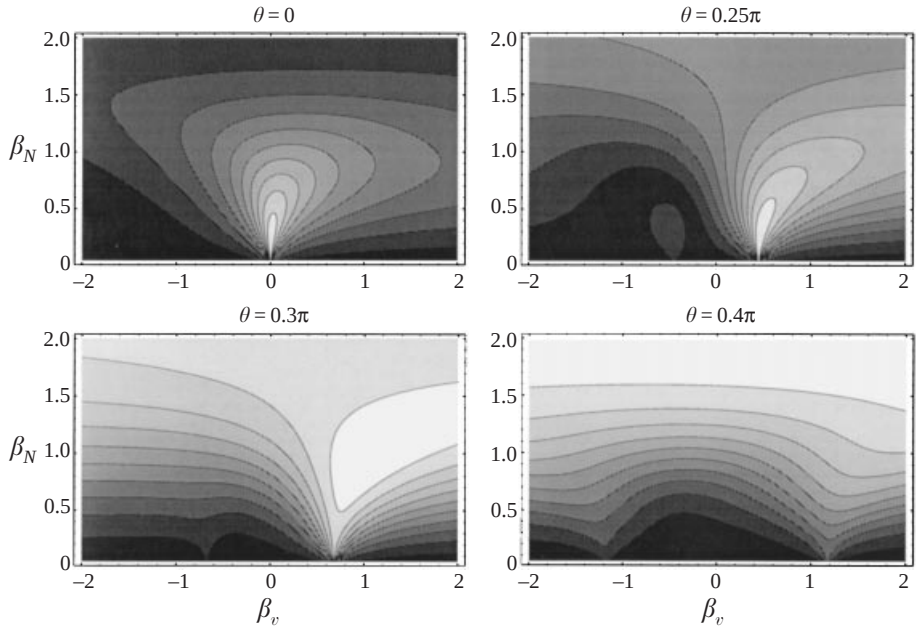

FIGURE 8. Contours of κ_v at different θ values ($M = 2$).

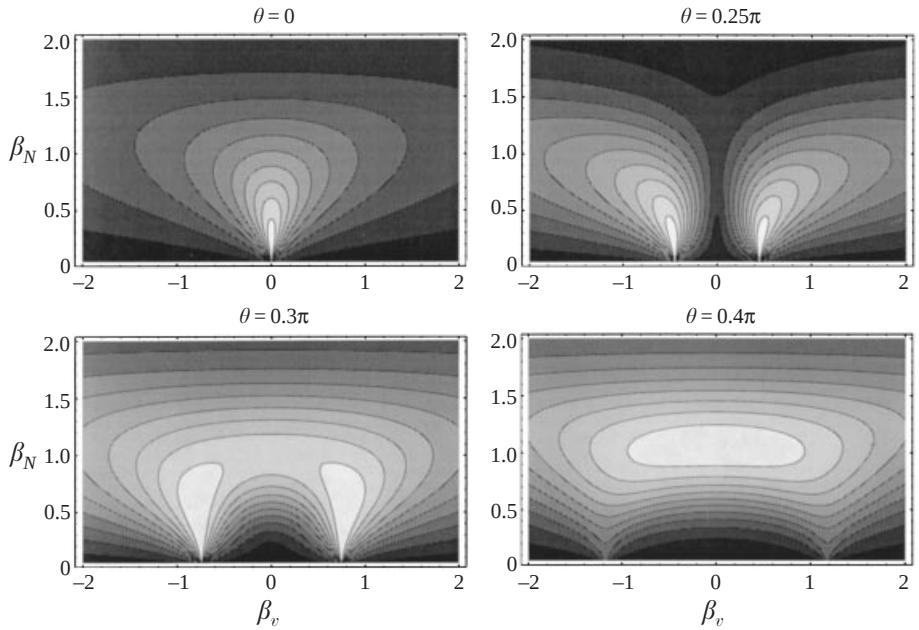

FIGURE 9. Contours of κ_e at different θ values ($M = 2$).

as M increases. As is indicated by figure 5, the receptivity appears to be particularly effective when $\theta = 0, \pi/2$. We thus examine more closely how the Mach number affects the coupling for these two incidence directions. The results are presented in figure 7(a, b), which shows that the coupling increases with M.

We now discuss the results for the supersonic regime. First note that the positive

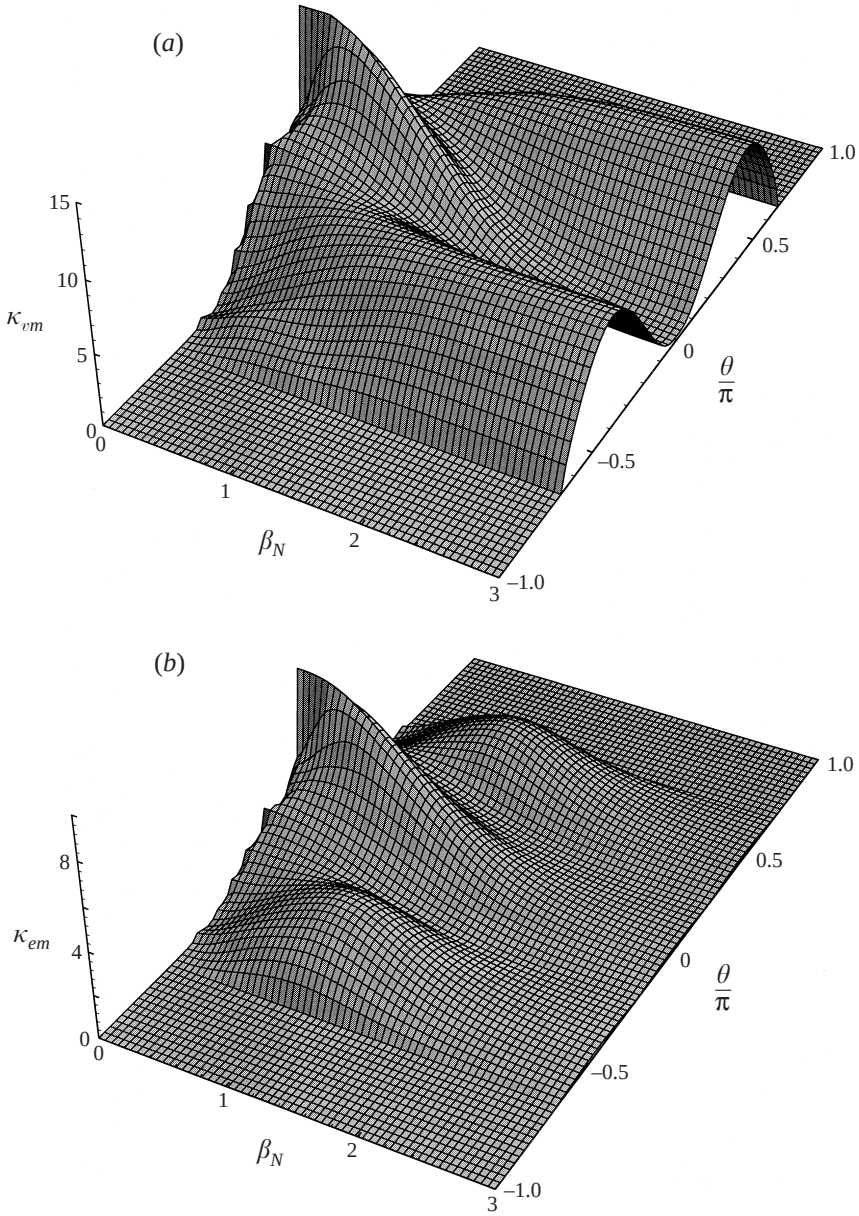

FIGURE 10. Variation of (*a*) κ_{vm} and (*b*) κ_{em} with respect to θ and β_N. $M = 2$.

condition for f_{TS} imposes a cut-off on θ, namely $|\theta| < \pi - \cos^{-1}(1/M)$; see (4.13). Figure 8 shows the contours of κ_v as a function of β_N and β_v for different values of θ with $M = 2.0$. The maximum of κ_v occurs at the small-β_N limit when θ is close to zero, and moves to the large-β_N limit when θ becomes large. However, unlike the subsonic regime the small-β_N limit does not correspond to (nearly) planar waves anymore, but rather represents oblique waves propagating along the surface of the Mach cone. A distinctive feature of these contours is the existence of cusps (one at $\theta = 0$ and two at $\theta \neq 0$ (or π)), about which the contours cluster. The appearance of the cusps is due to the fact that as $\beta_N \to 0$, D_v vanishes at $\beta_v = \pm\beta_s$ (see (2.52)),

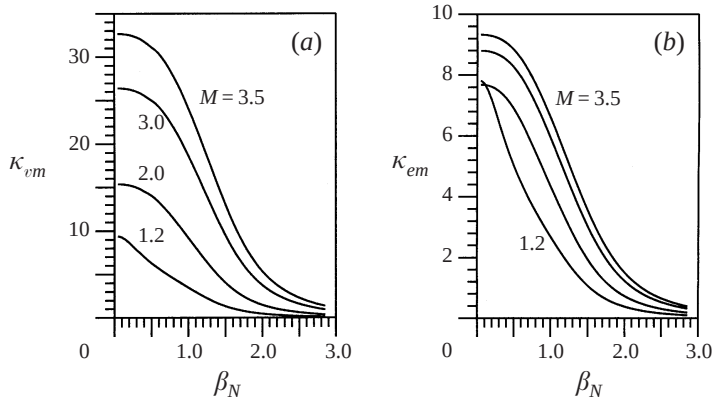

FIGURE 11. (*a*) κ_{vm} and (*b*) κ_{em} vs. β_N for the parallel incident sound ($\theta = 0$) at different Mach numbers $M = 1.2$, 2.0, 3.0, 3.5.

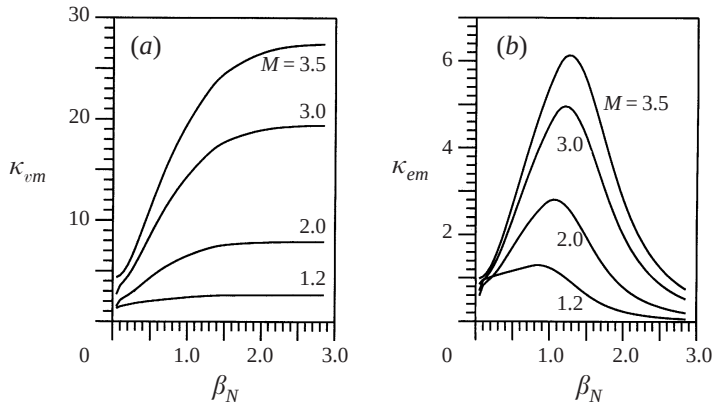

FIGURE 12. (*a*) κ_{vm} and (*b*) κ_{em} vs. β_N for the nearly perpendicular incident sound ($\theta = 2\pi/5$) at different Mach numbers $M = 1.2$, 2.0, 3.0, 3.5.

which means that the problem is somewhat 'singular' in the limit $(\beta_v, \beta_N) \to (\pm\beta_s, 0)$. Note also that for very small β_N (and hence small α_N), non-parallelism may affect the leading-order dispersion relation so that the triple-deck description may cease to be valid. In the present paper we avoid this singular limit by restricting $\beta_N > 0.05$. Contours of κ_e are displayed in figure 9, where the cusps appear for the same reason. Unlike the subsonic regime, κ_e attains its maximum at some finite β_N when θ is large.

The perspective plots in figure 10(*a*, *b*) illustrate how κ_{vm} and κ_{em} vary with β_N and θ. We can conclude that (*a*) if the incident sound is parallel to the free stream, both the acoustic–vorticity and acoustic–entropy interaction favours the excitation of the T–S waves which travel along the Mach cone and have long streamwise and spanwise wavelengths, and (*b*) if the sound is incident (nearly) perpendicular to the wall, then the entropy–vorticity interaction generates a band of oblique waves of finite wavelengths, while the acoustic–vorticity interaction tends to generate highly oblique waves. Again the incidence directions at which the sound is most effective in provoking T–S waves are centred at $\theta = 0,\ \pi/2$. In figures 11 and 12, we show κ_{vm} and κ_{em} at $\theta = 0, 0.4\pi$ for different values of M. Clearly the receptivity becomes more effective as M increases.

6.2. *Results for the isotropic free-stream turbulence*

The calculation of the T–S wave spectra requires the parameter R_Λ. Lacking the relevant data for the compressible flows, we use the data from the low-speed experiments of Westin *et al.* (1994), who took special measures to produce nearly isotropic free-stream turbulence, and carefully documented its characteristics, including the integral scale, the longitudinal energy spectrum, etc. The typical R_Λ varies from 2000 to 4000. We choose $R_\Lambda = 3000$. At fixed M and θ, the spectra $\Phi_{11}^{(v)}$ and $\Phi_{11}^{(e)}$ are two-dimensional functions of β_N and f_s (or equivalently α_{TS}). Since our interest is in the case where a single sound wave interacts with a broad turbulence spectrum, we fix $f_s = 2 \times 10^{-4}$, which corresponds to the 'upper limit' of the frequency range where the turbulence energy concentrates, and examine the 'composition' of the resulting T–S waves at different incident angles of the sound.

For the case $M = 0.5$, the spectra of the T–S waves at different θ are shown in figure 13(a, b). Interestingly, for all incident angles the most predominant response to the sound–vorticity interaction is a band of oblique waves centred at a finite β_N. These is in contrast to the result for a single component (cf. figure 5a), and the difference is due to the spectral composition of various components in the free stream, which is not accounted for by κ_v. The sound–entropy interaction, on the other hand, provokes a band of T–S waves centred at the planar modes; see figure 13(b), which also indicates that the optimal incident sound is the one travelling parallel to the free stream. But further calculations (not presented here) show that for smaller Mach numbers a sound wave travelling against, or perpendicular to, the free stream can be as effective.

The results for the supersonic regime ($M = 2.0$) are given in figure 14(a, b). For both sound-vorticity and sound-entropy interactions, the major composition of the response is a band of oblique T–S waves. But for the former, there exist three effective incident angles while for the latter there is only one.

6.3. *Further comments*

Our theoretical results show that a sound wave can generate T–S waves by interacting with a convecting gust (either a single component or in form of broad-spectrum turbulence). The magnitude of the T–S waves could be substantial in the subsonic boundary layer of moderate Mach number and even more so in supersonic flows. For instance, at $M = 0.3$, $\kappa_{vm} \approx 0.33$ and $\kappa_{em} \approx 0.9$ (at $\theta = 0$) according to figure 6. These give $C_V = 0.33$ $C_E = 0.9$, for the case where a sound wave of frequency $f_s = 10^{-4}$ interacts with a gust with a fluctuation level of 1% say,† implying that the intensity of the exited two-dimensional T–S wave would be comparable with that of the acoustic fluctuation. The T–S wave has a frequency $f_{TS} \approx 2.7 \times 10^{-5}$, while its neutral Reynolds number $R = 4 \times 10^5$, as can be estimated by using (4.11) and (4.13). At $M = 2$, $\kappa_{vm} \approx 15$ (see figure 11a), suggesting that the T–S wave amplitude would be an order of magnitude larger.

For the low-speed boundary layer, the present receptivity is weak. Indeed in the incompressible limit, the coupling coefficients, as calculated by the present method, vanish. However, the general idea outlined in § 2 is still valid. In fact, the actual coupling coefficient is not exactly zero, but is 'exponentially small' in *the asymptotic sense*. Exponentially small coupling also occurs in other receptivity mechanisms too, for example in the leading-edge receptivity (Goldstein 1983). Since the Reynolds

† The latest experiments of Dietz (1999) show that linear approximation for the gust is valid up to turbulence level of $\epsilon = 1\%$.

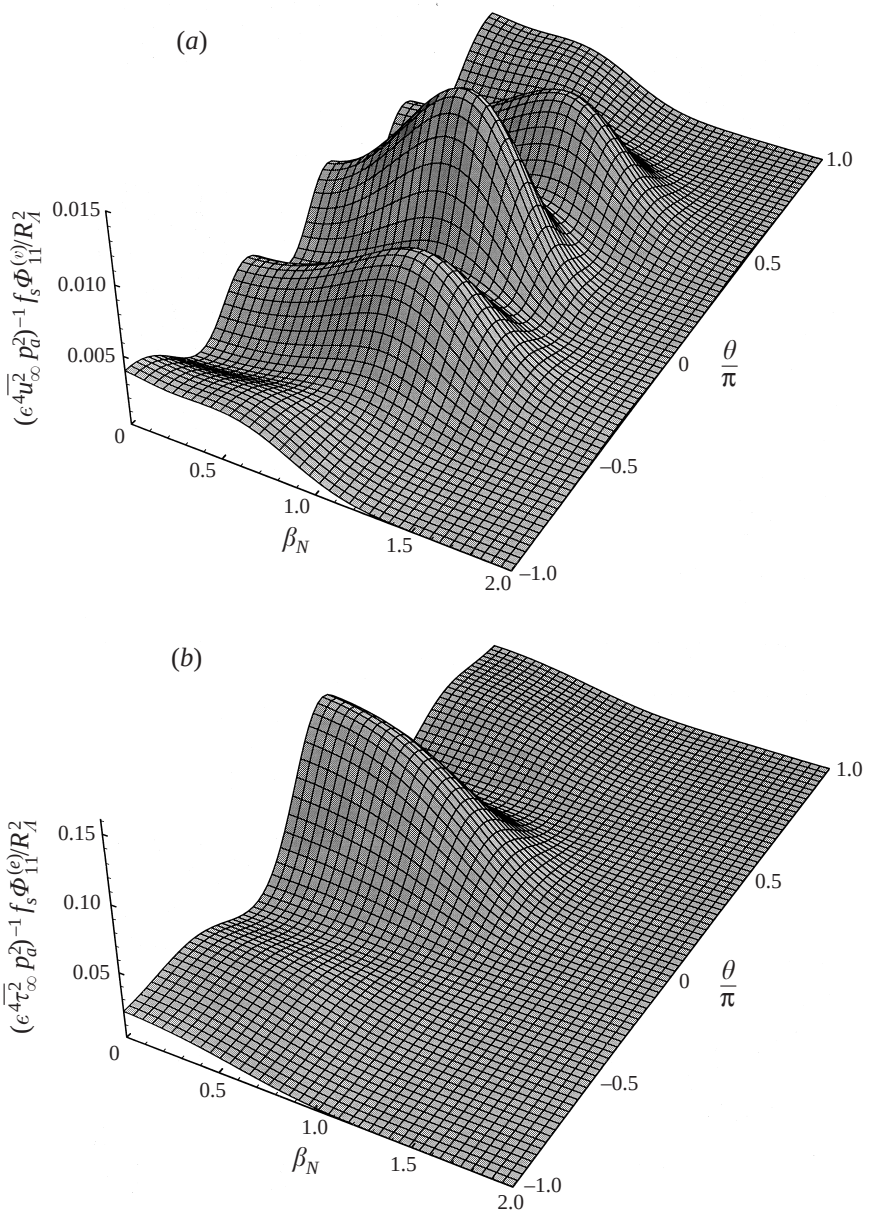

FIGURE 13. The spectrum of the T–S waves generated by isotropic turbulence in the subsonic regime ($M = 0.5$): (*a*) $\Phi_{11}^{(v)}$ and (*b*) $\Phi_{11}^{(e)}$ vs. β_N and θ.

number in practice is not very large, such an 'exponentially small' coupling may well turn out to be not so small in the *numerical sense*. If that is the case, the present mechanism may play a role in the incompressible boundary layer. In order to estimate the coupling in that case, one has to investigate the exponentially small signature of the gust within the boundary layer.

It appears that there are at least three distinctive receptivity mechanisms: the leading-edge adjustment (Goldstein 1983), the local inhomogeneity scattering (Goldstein 1985; Ruban 1984; Duck *et al.* 1996) and the present acoustic–gust interaction,

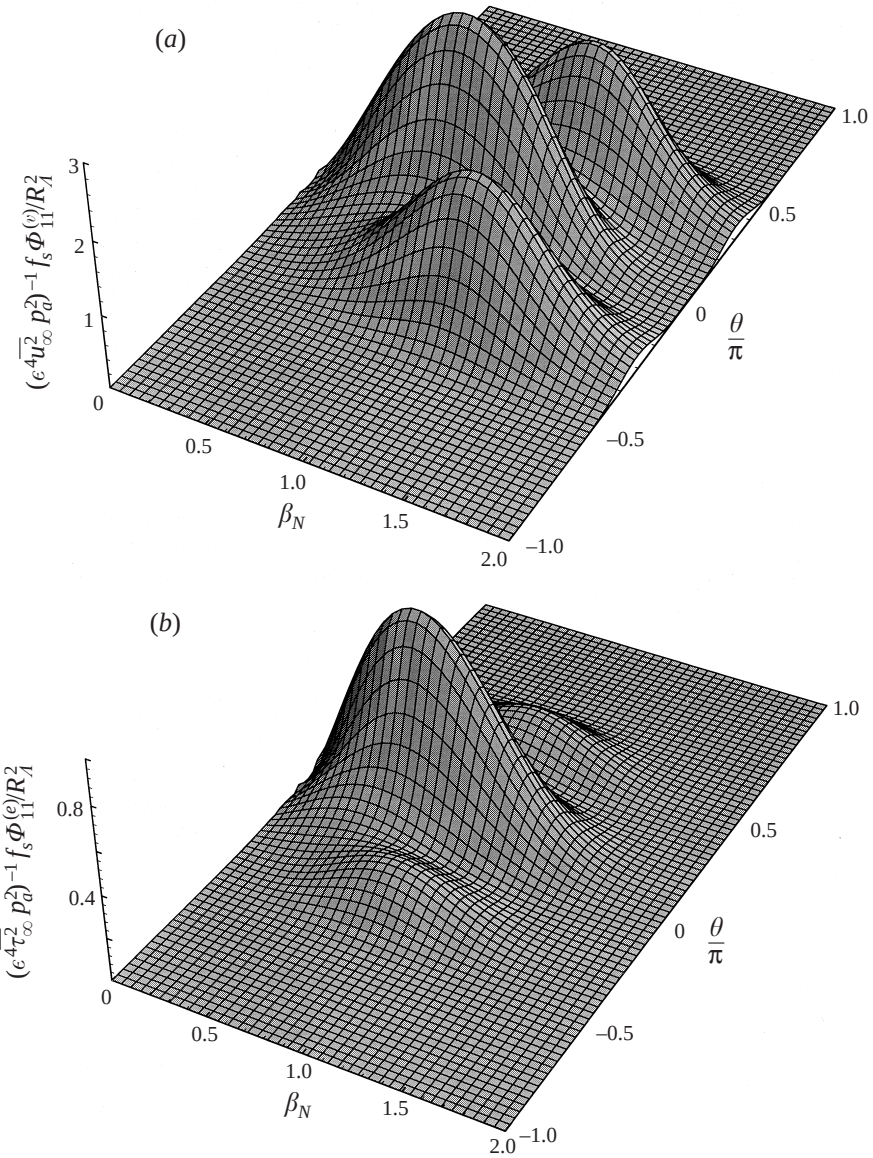

FIGURE 14. The spectrum of the T–S waves generated by isotropic turbulence in the supersonic regime ($M = 2$): (*a*) $\Phi_{11}^{(v)}$ and (*b*) $\Phi_{11}^{(e)}$ vs. β_N and θ.

each of which leads to generation of T–S waves. At the present time, there exist no relevant experimental data with which our results can be compared. Nevertheless it is possible for us to made a few suggestions about how experiments might be conducted so as to check at least some of the theoretical predictions.

As was indicated earlier, in order to verify directly the results in § 4, it is necessary to introduce a well-defined gust. The experiments of Dietz (1999) show that a single-frequency gust can be generated in a well-controlled manner by vibrating a ribbon in the free stream. Now if at the same time, a sound wave of appropriate frequency is applied to interact with the gust, detectable T–S waves may be excited. The difficulty

of course is that the experiments must be conducted at relatively high speeds at which the compressible effect is appreciable.

Another possible model for a gust is the Kármán vortex street, which may be generated from a cylinder inserted in the free-stream. Vortices are shed at a certain frequency and convected downstream to form a periodic pattern in the streamwise direction. (The convection velocity would be close to the free-stream velocity if the vorticity is weak.) An infinite array of point vortices may be used as a model for the street. The analysis in § 3 can be readily extended to this case so that a meaningful comparison could be made.

In a boundary layer where the convecting gust is of true turbulent nature, our theory shows that a deterministic sound wave can interact with the relevant components in the gust to excite a spectrum of T–S waves, which then become dominant downstream. Experimentally, the relevant quantities to measure are the mean-square values and the two-point covariances from which one can determined the T–S wave spectrum via Fourier transform. These quantities can be predicted theoretically as long as we know the spectrum tensor of the velocity fluctuation and the spectrum of the temperature fluctuation in the free stream. From both the experimental and theoretical point view, it is advantageous to create the standard free-stream condition where the turbulence is (nearly) isotropic as in Westin *et al.* (1994), since in this case the free-stream turbulence is completely characterized by the longitudinal energy spectrum function $E_1(k)$; this is the only input that the theory requires the experiments to provide in advance.

The suitable Mach number range for conducting such experiments probably is $0.3 < M < 0.8$. This is because in this range the receptivity is already strong enough and on the other hand one can avoid the transonic complications as well as shocks which would occur at supersonic speeds. Clearly, performing these experiments is a major challenge. It is our hope that the theoretical results in the present paper will provide useful guidance as well as necessary stimulus for further laboratory investigations.

The author would like to thank Professor J. T. Stuart, Dr S. J. Cowley and Professor M. Gaster for helpful discussion, and Dr M. E. Goldstein for encouragement. Thanks are also due to Dr L. Zabieski for his assistance with computer graphics, and to the referees for their detailed comments and suggestions, which have led to improvement of the present work.

REFERENCES

Aizin, L. B. & Polyakov, J. H. 1979 Acoustic generation of Tollmien–Schlichting waves over local unevenness of surface immersed in streams. *Preprint 17*. Akad. Nauk USSR Siberian Div., Inst. Theor. Appl. Mech. Novosibirsk (in Russian).

Batchelor, G. K. 1953 *The Theory of Homogeneous Turbulence*. Cambridge University Press.

Bodonyi, R. J., Welch, W. J. C., Duck, P. W. & Tadjfar, M. 1989 A numerical study of the interaction between unsteady free-stream disturbances and localized variations in surface geometry. *J. Fluid Mech.* **209**, 285–308.

Choudhari, M. 1993 Boundary-layer receptivity due to distributed surface imperfections of a deterministic or random nature. *Theor. Comput. Fluid Dyn.* **4** (3), 101.

Choudhari, M. 1994 Distributed acoustic receptivity in laminar flow control configurations. *Phys. Fluids* **6**, 489–506.

Choudhari, M. 1996 Boundary-layer receptivity to three-dimensional unsteady vortical disturbances in free stream. *AIAA Paper* 96-0181.

Choudhari, M. & Streett, C. L. 1992 A finite Reynolds number approach for the prediction of boundary-layer receptivity in localized regions. *Phys. Fluids* **4**, 2495–2514.

Chu, B.-T. & Kovasznay, L. S. G. 1958 Nonlinear interactions in a viscous heat-conducting compressible gas. *J. Fluid Mech.* **3**, 494–514.

Crouch, J. D. 1992 Localized receptivity of boundary layers. *Phys. Fluids* **4**, 1408–1414.

Crouch, J. D. 1994 Distributed excitation of Tollmien–Schlichting waves by vortical free-stream disturbances. *Phys. Fluids* **6**, 217–223.

Dietz, A. J. 1999 Local boundary-layer receptivity to a convected free-stream disturbance. *J. Fluid Mech.* **378**, 291–317.

Duck, P. W., Ruban, A. I. & Zhikharev, C. N. 1996 Generation of Tollmien–Schlichting waves by free-stream turbulence. *J. Fluid. Mech.* **312**, 341–371.

Goldstein, M. E. 1978 Unsteady vortical and entropic distortions of potential flows round arbitrary obstacles. *J. Fluid Mech.* **89**, 433–468.

Goldstein, M. E. 1979 Turbulence generated by the interaction of entropy fluctuations with non-uniform mean flows. *J. Fluid Mech.* **93**, 209–224.

Goldstein, M. E. 1983 The evolution of Tollmien–Schlichting waves near a leading edge. *J. Fluid Mech.* **127**, 59–81.

Goldstein, M. E. 1985 Scattering of acoustic waves into Tollmien–Schlichting waves by small streamwise variations in surface geometry. *J. Fluid Mech.* **154**, 509–529.

Goldstein, M. E. & Hultgren, L. S. 1987 A note on the generation of Tollmien–Schlichting waves by sudden surface-curvature change. *J. Fluid. Mech.* **181**, 519–525.

Goldstein, M. E. & Hultgren, L. S. 1989 Boundary layer receptivity to long-wave free-stream turbulence. *Ann. Rev. Fluid Mech.* **21**, 138.

Goldstein, M. E., Leib, S. J. & Cowley, S. J. 1987 Generation of Tollmien–Schlichting waves on interactive marginally separated flows. *J. Fluid Mech.* **181**, 485–517.

Goldstein, M. E., Sockol, P. M. & Sanz, J. 1983 The evolution of Tollmien–Schlichting waves near a leading edge. Part 2. Numerical determination of amplitudes. *J. Fluid Mech.* **129**, 443–453.

Gulyaev, A. N., Kozlov, V. E., Kuznetson, V. R., Mineev, B. I. & Sekundov, A. N. 1989 Interaction of laminar boundary layer with external turbulence. *Izv. Akad. Nauk SSSR Mekh. Zhid. Gaza* **6**, 700–710.

Haddad, O. M. & Corke, T. C. 1998 Boundary layer receptivity to free stream sound on parabolic bodies. *J. Fluid Mech.* **368**, 1–26.

Hall, P. & Smith, F. T. 1982 A suggested mechanism for nonlinear wall roughness effects on high Reynolds number flow stability. *Stud. Appl. Maths* **66**, 241–265.

Hall, P. & Smith, F. T. 1984 On the effects of non-parallelism, three-dimensionality and mode interaction in nonlinear boundary-layer stability. *Stud. Appl. Maths* **71**, 91–120.

Hammerton, P. W. & Kerschen, E. J. 1996 Boundary layer receptivity for a parabolic leading edge. *J. Fluid Mech.* **310**, 243–267.

Hammerton, P. W. & Kerschen, E. J. 1997 Boundary layer receptivity for a parabolic leading edge. Part 2. The small-Strouhal number limit. *J. Fluid Mech.* **353**, 205–220.

Hinze, J. O. 1959 *Turbulence*. McGraw-Hill.

Hunt, J. C. R. 1973 A theory of turbulent flow round two-dimensional bluff bodies. *J. Fluid Mech.* **61**, 625–706.

Hunt, J. C. R & Graham, J. M. R 1978 Free-stream turbulence near plane boundaries. *J. Fluid Mech.* **84**, 209–235.

Kachanov, Y. S., Kozlov, V. V. & Levchenko, V. Y. 1978 Occurrence of Tollmien–Schlichting waves in the boundary layer under the effect of external perturbations. *Izv. Akad. Nauk SSSR Mekh. Zhid. Gaza.* **5**, 85 (English translation: *Fluid Dyn.* **13**, 704).

Kendall, J. M. 1985 Experimental study of disturbances produced in pre-transitional laminar boundary layer by weak free stream turbulence. *AIAA Paper* 85-1695.

Kendall, J. M. 1990 Boundary-layer receptivity to free-stream turbulence. *AIAA Paper* 80-1504.

Kerschen, E. J. 1991 Linear and nonlinear receptivity to vortical free-stream disturbances. In *Boundary Layer Stability and Turbulence* (ed. D. C. Reda, H. L. Reed & R. K. Kobayashi). ASME FED, vol. 114, pp. 43–48.

Kobayashi, R., Fukunishi, T., Nishikawa, T. & Kato, T. 1995 The receptivity of flat-plat boundary-layers with two-dimensional roughness elements to free-stream sound and control. In *Proc. IUTAM Symp. on Laminar-Turbulent Transition* (ed. R. Kobayashi), pp. 507–514. Springer.

Kosorygin, K. S., Radeztsky, R. H. Jr. & Saric, W. S. Laminar boundary-layer, sound receptivity and control. In *Proc. IUTAM Symp. on Laminar-Turbulent Transition* (ed. R. Kobayashi), pp. 517–524. Springer.

Kovasznay, L. S. G. 1953 Turbulence in supersonic flow. *J. Aero. Sci.* **20**, 657–682.

Kozlov, V. V. & Ryzhov, O. S. 1990 Receptivity of boundary layers: asymptotic theory and experiments. *Proc. R. Soc. Lond.* A **440**, 341.

Leehey, P. & Shapiro, P. J. 1980 Leading edge effect in laminar boundary layer excitation by sound. In *Proc. IUTAM Symp. on Laminar-Turbulent Transition*, pp. 321–331. Springer.

Luo, J. S. & Zhou, H. 1988 On the generation of Tollmien–Schlichting waves in the boundary layer of a flat plate by the disturbances in the free stream. *Proc. R. Soc. Lond.* A **413**, 351–367.

Mack, L. M. 1984 Boundary-layer linear stability theory. *AGARD Rep.* 709.

Morkovin, M. V. 1969 Critical evaluation of transition from laminar to turbulent shear layers with emphasis on hypersonically travelling bodies. US Air Force Flight Dynamics Laboratory, Wright Patterson Air Force Base, Ohio, AFFDL-TR, 68–149.

Reshotko, E. 1976 Boundary layer stability and transition. *Ann. Rev. Fluid Mech.* **8**, 311.

Ruban, A. I. 1983 Nonlinear equation for the amplitude of Tollmien–Schlichting waves in the boundary layer. *Izv. Akad. Nauk. SSSR Mekh. Zhid. Gaza* **6**, 60–67.

Ruban, A. I. 1984 On Tollmien–Schlichting wave generation by sound. *Izv. Akad. Nauk. SSSR Mekh. Zhid. Gaza* **5**, 44 (English Translation: *Fluid Dyn.* **19**, 709–716 (1985)).

Ryzhov, O. S. & Timofeev, S. V. 1995 Interaction of a potential vortex with a local roughness on a smooth surface. *J. Fluid Mech.* **287**, 21–58.

Saric, W. S., Wei, W. & Rasmussen, B. K. 1995 Effect of leading edge on sound receptivity. In *Proc. IUTAM Symp. on Laminar-Turbulent Transition* (ed. R. Kobayashi), pp. 413–420. Springer.

Smith, F. T. 1979*a* On the nonparallel flow stability of the Blasius boundary layer. *Proc. R. Soc. Lond.* A **366**, 91–109.

Smith, F. T. 1979*b* Nonlinear stability of boundary layers for disturbances of various sizes. *Proc. R. Soc. Lond.* A **368**, 573–589.

Smith, F. T. 1989 On the first-mode instability in subsonic, supersonic or hypersonic boundary layers. *J. Fluid Mech.* **198**, 127–153.

Terent'ev, E. D. 1981 The linear problem of a vibrator in a subsonic boundary layer. *Prikl. Math. Mech.* **45** (6), 1049–1055.

Westin, K. J. A., Boiko, A. V., Klingmann, B. G. B., Kozlov, V. V. & Alfredsson, P. H. 1994 Experiments in a boundary layer subjected to free stream turbulence. Part I. Boundary layer structure and receptivity. *J. Fluid Mech.* **281**, 193–218.

Zhigulev, V. N. & Tumin, A. M. 1987 *Origin of Turbulence*. Nauka, Novosibirsk.